

Learning efficient backprojections across cortical hierarchies in real time

Kevin Max¹, Laura Kriener¹, Garibaldi Pineda García²,
Thomas Nowotny², Ismael Jaras¹, Walter Senn¹, and Mihai A. Petrovici¹

¹Department of Physiology, University of Bern, Switzerland

²School of Engineering and Informatics, University of Sussex, Brighton, United Kingdom

February 5, 2024

Abstract

Models of sensory processing and learning in the cortex need to efficiently assign credit to synapses in all areas. In deep learning, a known solution is error backpropagation, which however requires biologically implausible weight transport from feed-forward to feedback paths. We introduce Phaseless Alignment Learning (PAL), a bio-plausible method to learn efficient feedback weights in layered cortical hierarchies. This is achieved by exploiting the noise naturally found in biophysical systems as an additional carrier of information. In our dynamical system, all weights are learned simultaneously with always-on plasticity and using only information locally available to the synapses. Our method is completely phase-free (no forward and backward passes or phased learning) and allows for efficient error propagation across multi-layer cortical hierarchies, while maintaining biologically plausible signal transport and learning. Our method is applicable to a wide class of models and improves on previously known biologically plausible ways of credit assignment: compared to random synaptic feedback, it can solve complex tasks with fewer neurons and learn more useful latent representations. We demonstrate this on various classification tasks using a cortical microcircuit model with prospective coding.

1 Introduction

The two fields of deep learning and neuroscience remain at vastly different levels in the description of their respective subjects. While deep learning has made great leaps in terms of applicability and real-world usage in the past decade, the study of biological neural systems has revealed a plethora of different brain areas, connection types, cell types, and neuron as well as system states. Currently, no clear organization scheme of computations and information transfer in the brain is known, and the question of how artificial neural networks (ANNs) are related to models of the cortex remains an active field of research [1–3].

However, progress is being made in bridging the gap between these two fields [1, 2, 4–12]. In particular, important similarities between cortical and artificial information processing have been highlighted: as in the cortex [13], most ANN architectures process information hierarchically. Neural activity is modulated through learning, i.e. long-term adaptation of synaptic weights. However, it is currently unclear how weights are adapted across the cortex in order to competently

solve a task. This is commonly referred to as the credit assignment problem, where neuroscience may learn from deep learning [2, 14].

In the case of ANNs, a solution to this problem is known: currently, error backpropagation (BP) [15, 16] is the gold standard. However, BP has several biologically implausible requirements. ANNs trained with BP operate in distinct, alternating forward (inference) and backward (learning) phases. Between phases, network activities need to be buffered – i.e., information is processed non-locally in time. Furthermore, error propagation occurs through weights which need to be mirrored at synapses in different layers (weight transport problem).

In order to explain credit assignment for analog, physical computing (in the cortex or on neuromorphic hardware), physically plausible architectures and algorithms are therefore needed. We assume such dynamical systems to operate in continuous time. Ideally, physical systems are able to learn from useful instructive signals at all times, using only information which is locally available in space and time. Crucially, all physical systems have inherent sources of noise – in the form of stochastic activity, noisy parameters or intrinsic fluctuations of electrical and chemical signals. The theory we propose makes use of neuronal noise as an additional carrier of information, instead of treating it as a nuisance.

For efficient credit assignment, errors need to be propagated from higher to lower areas in the hierarchy. Broadly, approaches can be categorized into methods with fixed feedback connections (feedback alignment, FA [10, 17]), bio-plausible approximations to BP [18–21], or alternative cost minimization schemes [22–25]. In this work, we introduce a method in the second category, related to the top-down weight alignment method of Ref. [21], which itself is based on previous insights on cost minimization in difference target propagation [24].

Our theory improves on existing literature in several ways: We propose a fully dynamical system with efficient always-on plasticity. The neuronal and weight continuous-time dynamics model properties of physical substrates and plasticity is enabled for all synapses and at all times. In agreement with biological plausibility, our method allows for efficient learning without requiring wake-sleep phases or other forms of phased plasticity implemented in many other models of learning in the cortex [6, 8, 26–32]. Our method is based on modeling of biologically plausible signal transport, and the learning mechanism incorporates bio- and hardware-plausible computations; all dynamics and plasticity rules are fully local in time and space.

2 Results

2.1 Learning of efficient backprojections

We describe our theory in a rate-based coding scheme. The architecture is modeled with layers $\ell = 1 \dots N$ of leaky-integrator neurons as

$$\tau^{\text{eff}} \dot{\mathbf{u}}_\ell = -\mathbf{u}_\ell + \mathbf{b}_\ell + \mathbf{W}_{\ell, \ell-1} \mathbf{r}_{\ell-1} + \mathbf{e}_\ell + \boldsymbol{\xi}_\ell. \quad (1)$$

In this description, the somatic potential \mathbf{u}_ℓ integrates neuron bias \mathbf{b}_ℓ , the bottom-up input rate $\mathbf{r}_{\ell-1}$ weighted with $\mathbf{W}_{\ell, \ell-1}$, and the local error \mathbf{e}_ℓ . The integration time scale is set by the effective membrane time constant τ^{eff} , defined by conductance and capacitance of the cell. An essential ingredient is the noise component $\boldsymbol{\xi}_\ell$.

Our theory integrates the prospective coding mechanism of Latent Equilibrium [9], which solves the relaxation problem of slow physical substrates, which disrupts inference as well as learning (see Methods). This is achieved by calculating the neural output from the prospective voltage $\check{\mathbf{u}} := \mathbf{u} + \tau^{\text{eff}} \frac{d\mathbf{u}}{dt}$ for all neurons. As a result, the rates $\mathbf{r}_\ell := \varphi(\check{\mathbf{u}}_\ell)$ follow the neuron’s inputs quasi-instantaneously.

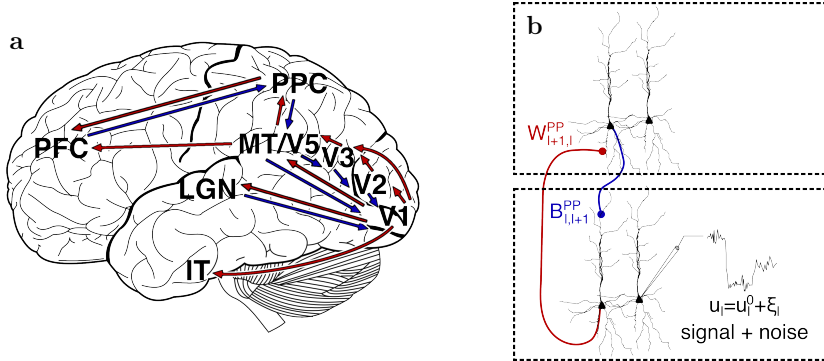


Figure 1: Sensory processing over cortical hierarchies. **a:** Brain areas in the visual pathway beyond the primary visual cortex (V1). Information is propagated to higher areas (red arrows) such as V2, V4, the medial temporal (MT) area, and beyond. In order to assign credit, feedback information from higher level areas needs to be propagated top-down (blue arrows). Adapted from [37, 38]. **b:** Pyramidal cells as functional units of sensory processing and credit assignment. Top-down and bottom-up projections preferentially target different dendrites. Due to stochastic dynamics of individual neurons, noise is added to the signal.

The central question of cortical credit assignment is how the error e_ℓ is calculated, given an error signal in a higher area, $e_{\ell+1}$, and how this error signal is used to adjust bottom-up weights. Plenty of solutions to this question have been proposed [12]. Here, we focus on theories which can be formulated such that forward weights are updated as $\dot{\mathbf{W}}_{\ell,\ell-1} \propto e_\ell \mathbf{r}_{\ell-1}^T$. Under this scheme, several theories for bio-plausible error transport exist [6, 8, 9, 23, 24, 31]. They have in common that errors in a higher layer $e_{\ell+1}$ are propagated down through feedback (top-down) weights $\mathbf{B}_{\ell,\ell+1}$ to form errors in a given layer e_ℓ .

Typically, symmetric weights are assumed, such that $\mathbf{B}_{\ell,\ell+1} = [\mathbf{W}_{\ell+1,\ell}]^T$ [6, 8, 31, 33]. Alternatively, learning schemes apply $\dot{\mathbf{B}}_{\ell,\ell+1} = [\dot{\mathbf{W}}_{\ell+1,\ell}]^T$ [4, 11, 18, 34], leading to weight alignment. Both assumptions relate the above error propagation schemes to classical backpropagation, where $e_\ell = \varphi' \cdot [\mathbf{W}_{\ell+1,\ell}]^T e_{\ell+1}$. However, this assignment of weights (or weight updates) implies that top-down synapses in layer ℓ must adapt to the bottom-up synapses in layer $\ell + 1$. This issue of how two spatially distant synapses (e.g. across cortical areas) can maintain similar weights when one of them is learning is known as the *weight transport problem*.

A proposed solution is replacing $\mathbf{B}_{\ell,\ell+1}$ with a random, fixed weight matrix (known as feedback alignment, FA [10]). However, FA has been shown to solve credit assignment inefficiently, and does not scale well to complex problems [17, 20, 35, 36]. We are therefore motivated to learn top-down weights such that credit assignment is improved compared to random feedback with layer-wise connections. Furthermore, we would like to learn all weights $\mathbf{B}_{\ell,\ell+1}$ simultaneously, and in a way which does not interrupt feed-forward inference or learning of bottom-up weights.

The general method we propose is explained in the following (see Fig. 1). An input signal $\mathbf{r}_0(t)$ (‘data’) is presented to the neurons in the lowest layer for the duration of a presentation time T_{pres} . To reflect the inherent stochasticity of biological neurons subject to synaptic noise, thermal activity and probabilistic firing, high-frequency noise ξ_ℓ with a time constant τ_ξ is modeled at every neuron. This noise is accumulated across layers, and propagated on top of the data signal. The top-down projections carry this mixed signal back to the lower layers, and we exploit the auto-correlation between noise signals to learn the corresponding feedback synapses.

To learn the backwards weights, simple and only local computations need to be performed. At every top-down synapse $\mathbf{B}_{\ell,\ell+1}$, a high-pass filtered rate $\hat{\mathbf{r}}_{\ell+1}$ is computed, which extracts

been introduced with biological plausible (error) signal transport in mind. Each microcircuit is defined by layer-wise connected populations of two types of neurons, pyramidal cells and interneurons, see Fig. 2 and Methods. and Methods.

In contrast to the model defined by Ref. [8], which employs FA, we learn the backward connections using PAL with the scheme defined in Sec. 2.1. We consider noise in the hidden layers with a small amplitude compared to the corresponding somatic potentials. Synaptic plasticity of thus-far fixed weights $\mathbf{B}_{\ell,\ell+1}^{\text{PP}}$ is enabled through the learning rule Eq. (2). Finally, in order to preserve learning of feed-forward weights, we endow the update rule of $\mathbf{W}_{\ell,\ell-1}^{\text{PP}}$ with a low-pass filter with time constant τ_{o} . Note that all computations required for PAL can be performed locally by the corresponding synapse.

2.3 Experiments

2.3.1 Phaseless backwards weight alignment

We first demonstrate that PAL aligns top-down weights in cortical microcircuits with the theoretical result given by Eq. (3). We simulate the dendritic microcircuit model with three hidden layers, keeping the forward weights $\mathbf{W}_{\ell,\ell-1}^{\text{PP}}$ fixed while modeling noise in all hidden layers and learning all $\mathbf{B}_{\ell,\ell+1}^{\text{PP}}$ simultaneously. Top-down weights as well as lateral weights from interneurons to pyramidal cells are adapted fully dynamically during training.

Results are shown in Fig. 3, where the upper and lower row correspond to the two cases where neurons are active in their linear/non-linear regime. It is of interest to evaluate both of these regimes, as complex tasks cannot be solved with a fully linear network. Nevertheless, it is also not the case that all neurons are in the non-linear regime for all inputs; typically, there is a mixture of both states present in the network.

The first column shows the angle between top-down weights and Eq. (3), demonstrating good agreement with the theoretical expectation over all hidden layers. These backward weight configurations are useful, as they approximately align with the transpose of the forward weights; we show the corresponding alignment angle in the second column. Alignment of top-down weights with the transpose is much better in the linear regime, as $\varphi' = \mathbf{1}$. We hypothesize that the larger misalignment angle in the non-linear case is due to the data-specific learning of backwards weights (see Discussion).

In the third column, we show that errors propagated in a microcircuit with PAL approximately align with backpropagation. After each epoch of training the backprojections, we evaluate the model in its current state by introducing a teaching signal. This generates an error which propagates to all layers, and from which a forward weight update $\Delta\mathbf{W}_{\ell,\ell-1}^{\text{PP}}$ is constructed; see Methods for details. We compare $\Delta\mathbf{W}_{\ell,\ell-1}^{\text{PP}}$ of this microcircuit model to the weight updates $\Delta\mathbf{W}_{\ell,\ell-1}^{\text{BP}}$ in an ANN with backpropagation and equal feed-forward weights. The results demonstrate that PAL is able to propagate useful error signals through alignment of backward weights.

2.3.2 Teacher-student setup

To further demonstrate that PAL enables propagation of useful error signals, we turn to a simple teacher-student task. Plasticity is now enabled in forward synapses, too. A microcircuit model consisting of a chain of two neurons is trained with PAL and FA, and the ideal case of BP. A teaching signal is obtained from a similar two-neuron chain connected with fixed, positive weights. The task of the student is to adapt its weights to reproduce the input-output relationship.

In order to highlight an important shortcoming of FA, we initialize the student models with negative forward and backward weights. As shown in Fig. 4, a model trained with FA is not able to reproduce the teacher output and even has diverging weights. This is caused by the

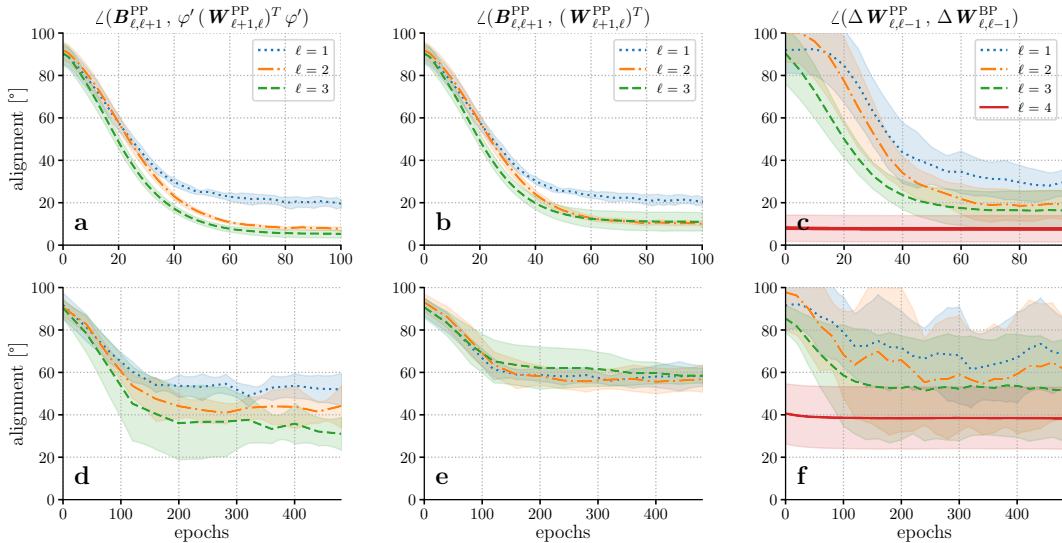


Figure 3: PAL aligns weight updates with backpropagation in deep networks. **a, b, c:** We train the backward projections in a deep microcircuit network with layer sizes [5-20-10-20-5] and sigmoid activation with no target present. All backward weights $\mathbf{B}_{\ell, \ell+1}^{PP}$ are learned simultaneously, while forward weights are fixed. Lines and shading show mean and standard deviation over 10 seeds. Weights are initialized as $\mathbf{W}^{PP} \sim \mathcal{U}[-1, 1]$, such that neurons are activated in their linear regime. The right column compares the *potential* forward weight updates generated from backpropagation using $\mathbf{B}_{\ell, \ell+1}^{PP}$ in the microcircuit model to those in an ANN with BP (see main text and Methods), where the instructive signal is provided by a teacher network with arbitrary forward weight configuration. **d, e, f:** Same as above, but with weights initialized in non-linear regime, $\mathbf{W}^{PP} \sim \mathcal{U}[-5, 5]$. Weight updates (f) are biased towards misalignment due to the dendritic microcircuit model, see Methods.

wrong sign of the top-down weights: a positive error on the output layer is projected backwards through the negative synapse $\mathbf{B}_{1,2}^{PP}$. Thus, the weight $\mathbf{W}_{1,0}^{PP}$ to the hidden layer grows negatively, further increasing the disparity between teacher and student weights. PAL resolves this issue by approximately aligning $\mathbf{B}_{1,2}^{PP}$ with $\mathbf{W}_{2,1}^{PP}$, thereby learning backwards weights with correct sign (left column in Fig. 4). Note that as long as $\mathbf{B}_{1,2}^{PP}$ has not yet aligned, $\mathbf{W}_{1,0}^{PP}$ moves in the wrong direction, but as soon as $\mathbf{B}_{1,2}^{PP}$ switches sign, the forward weight is able to learn correctly.

2.3.3 Classification experiments

We now turn to more complex tasks and evaluate PAL on classification benchmarks, while still working with the biologically plausible microcircuits as the base model. Due to the complexity of simulating microcircuit models with full dynamics, we focus this evaluation on the computationally effective Yin-Yang task, and perform experiments on MNIST digit classification as a sanity check.

The Yin-Yang classification problem [42] is designed to be a computationally inexpensive task which nonetheless requires useful error signals to reach the lower layer of a network, i.e. is able to differentiate the error propagation quality between FA and BP or variants of it. ANNs trained with backprop can solve this task with as few as 30 hidden neurons (test error 2.4 ± 1.5 %) [42].

The microcircuit models with PAL achieve a test error of 4.0 ± 0.4 %, performing considerably better than microcircuits with fixed random feedback weights at 7.8 ± 2.4 % (Fig. 4, center column). This is reflected in the increased alignment between the transpose of forward and backward weights.

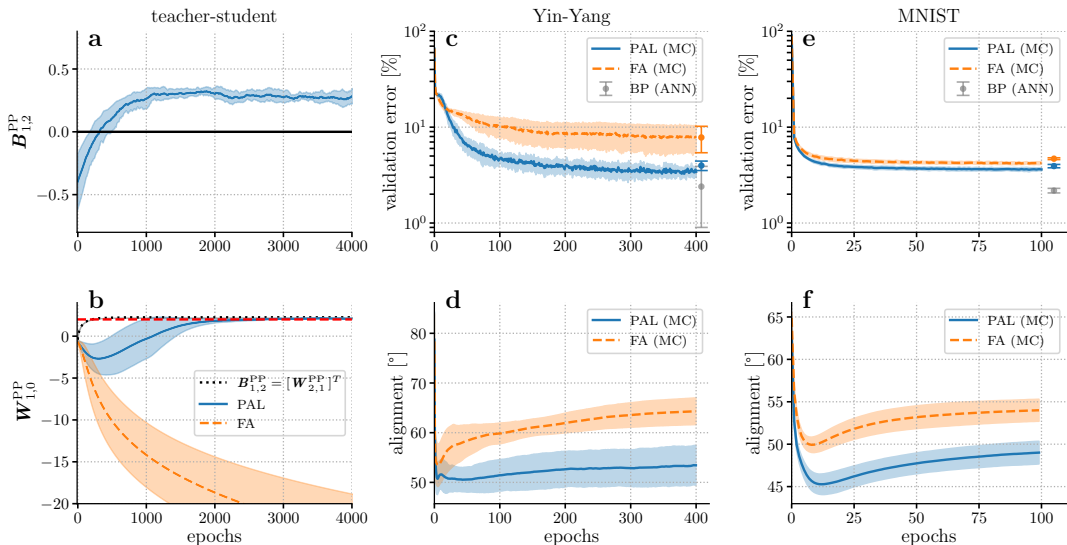


Figure 4: PAL improves learning on teacher-student and classification tasks compared to fixed random synaptic feedback. **a, b:** A chain of two neurons learns to mimic a teaching signal. The student neurons are initialized with negative weights and need to flip the sign. In particular, in order to achieve correct weights to the hidden neuron $\mathbf{W}_{1,0}^{PP}$, positive feedback weights are required. The teacher (red) has a positive weight. Results for student neuron chains are shown for PAL (blue) and FA (orange). The shading indicates mean and standard deviation over 10 seeds. Due to the wrong sign of the transported error, random synaptic feedback fails to solve the task, and weights diverge. The models trained with PAL start in a similar fashion; however, after sign flip (at about 500 epochs, see **a**), the error signal becomes useful, and $\mathbf{W}_{1,0}^{PP}$ converges to the weight of the teacher. As a control, we also show the ideal solution with weight transport, $\mathbf{B}_{1,2}^{PP} = (\mathbf{W}_{2,1}^{PP})^T$. **c, d:** Validation error during training and test errors for the Yin-Yang task (**c**) of the microcircuit model (MC) with network size [4-30-3]. For reference, we also show the test error in an ANN trained with BP with equal network size. The shading indicates mean and standard deviation over 10 seeds. **d:** Alignment angle between backwards weights $\mathbf{B}_{1,2}^{PP}$ and $(\mathbf{W}_{2,1}^{PP})^T$. While FA relies on alignment of forward weights, PAL improves on this by aligning the backward weights with the transpose of forward weights. **e, f:** Same as center column, but for the MNIST data set with network size [784-100-10]. Note that the increased performance cannot simply be attributed to the inclusion of noise, see Supplement.

We also perform the MNIST task with a similar setup (right panel in Fig. 4). In a similar vein to the Yin-Yang experiments, this single and small hidden layer is chosen as to highlight whether a good latent representation is formed. We achieve a final test error 3.9 ± 0.2 % using PAL and 4.7 ± 0.1 % with FA.

We highlight that our results were obtained by simulating a fully dynamical, recurrent and bio-plausible system with weight and voltage updates applied at every time step. This is in contrast to previous simulations using bio-plausible networks with recurrency, where simplified network dynamics were assumed for computational feasibility [8, 11, 43]. As a direct comparison, simulations on the MNIST task in Ref. [8] use the steady state approximation of voltage dynamics, and weight updates are calculated in two distinct steps. In effect, this simplifies the recurrent dynamics defined by Eq. (17) to those of an ANN with separate forward and backward phases and voltage buffering. Such approximations do not accurately reproduce the dynamics of recurrent physical networks, and we highlight that our results represent a significant step towards efficient bio-realistic microcircuit simulations.

2.3.4 Efficient credit assignment in deep networks

The previous analyses have shown that PAL can learn useful backprojections in dynamical systems. The simulations performed with microcircuit models stress the bio-plausibility of PAL. However, the microcircuit model (both with and without PAL) carries the issue that error signals decay with increasing hidden layer number (see Methods). PAL is designed to learn useful backprojections in deep hierarchies; in order to demonstrate the full capability of our method, we now relax our requirement for bio-plausible error transport and shift away from the dendritic microcircuit model.

We revisit the general leaky integrator model defined by Eq. (1), where errors are transported directly via $e_\ell = \varphi'(\tilde{\mathbf{u}}_\ell) \cdot \mathbf{B}_{\ell, \ell+1} e_{\ell+1}$.

We demonstrate the capability of PAL for credit assignment using the MNIST-autoencoder task (Figure 5) [20]. Autoencoders can be used to greatly compress an input image to a latent representation, in this case reducing down to a vector of dimension two. In order to decode such a representation, a successfully trained autoencoder network should show a separation of input of different classes in the latent space. To learn a well separated latent representation, suitable error signals need to travel through the whole network to train the encoder weights. We compare the performance of PAL with FA and its variant direct feedback alignment (DFA), where the feedback signal from the output layer is sent directly to all hidden layers [17, 44].

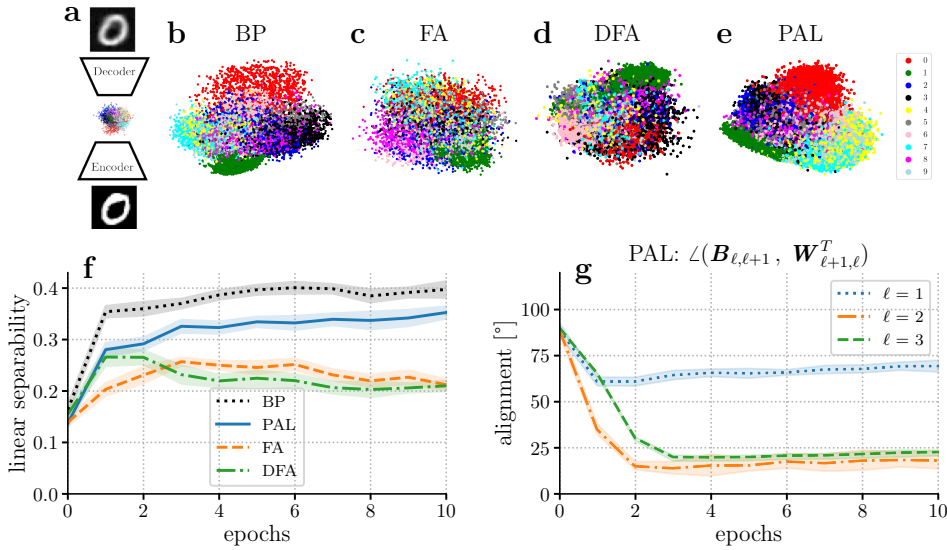


Figure 5: PAL learns useful latent representations, where feedback alignment fails to do so.

a: Encoder/decoder setup network with size [784-200-2-200-784]. MNIST digit dataset is fed into an encoder network with two output neurons. A stacked decoder network aims to reproduce the original input. **b-d:** Latent space activations after training. We show the activations after training in the two-neuron layer of one seed for all samples in the test set; colors encode the corresponding label. Backpropagation and PAL show improved feature separation compared to (direct) feedback alignment. **e:** Linear separability of latent activation. **f:** Alignment angle of top-down weights to all layers for the PAL setup (mean and standard deviation over 10 seeds). PAL is able adapt top-down weights while forward weights are also learned. Note that the layer $\ell = 1$ maps 200 neurons onto two in the forward direction, leading to many possible solutions in the backwards direction, and hence a larger alignment angle is to be expected.

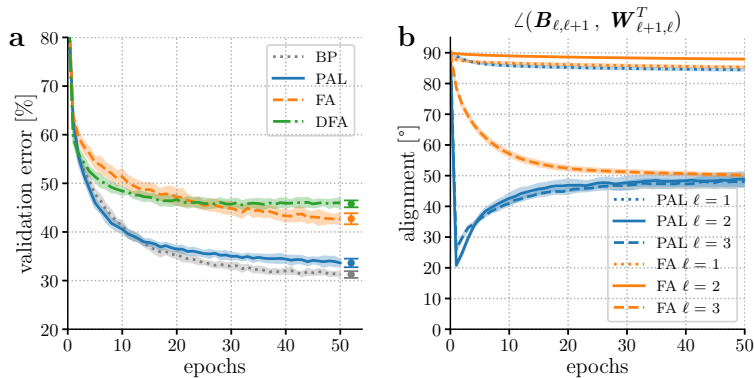


Figure 6: PAL outperforms (D)FA on CIFAR-10 using a continuous-time CNN. The network consists of four layers (Conv2d + MaxPool(2), Conv2d + MaxPool(2), dense, linear) with sigmoid activations, see Methods. **a:** Validation and test accuracies show that PAL outperforms FA and DFA on CIFAR-10. Noise is disabled for PAL during evaluation (val+test) in order to enable a fair comparison. Test accuracies are: BP 31.2 ± 0.7 %; PAL 33.9 ± 0.7 %; FA 42.7 ± 1.1 %; DFA 46.8 ± 0.7 %. **b:** Alignment between forward and backwards weights for PAL and FA for all layers. PAL is enabled for layers $\ell = 2, 3$ ($\ell = 1$ is a convolutional layer, for which PAL is not defined). All curves show mean and error over 10 seeds.

We evaluate the latent space separability by training a linear classifier. Results shown in Fig. 5 (e) demonstrate that networks trained with PAL achieve linear separability close to BP ((35.2 ± 1.2) % vs. (39.7 ± 1.6) %, respectively), while training with (direct) FA leads to significantly poorer feature separation at a test accuracy of (21.2 ± 1.0) % (DFA: (21.0 ± 1.0) %). Fig. 5 (f) shows that PAL is able to learn the transpose of forward weights across hidden layers.

Similarly, we show that PAL outperform (D)FA on CIFAR-10 using a continuous-time ConvNet (Fig. 6). PAL clearly outperforms random feedback by learning weights to a high degree of alignment.

3 Discussion

We have introduced PAL, a general method of learning backprojections in hierarchical, dynamical networks. Our theoretical results and simulations show that PAL provides online learning of forward and backward weights in a phaseless manner. As a general method, it is applicable to models where time-continuous activity is propagated, and approximately aligns feedback weights with those of backpropagation. PAL fulfills the requirements of learning and signal transport in physical systems: all necessary information is available locally in time and space.

In our evaluation, we have emphasized the biological plausibility of PAL as a model of sensory processing. PAL could be implemented in biological components; in particular, it explicitly exploits noise found in physical systems and makes use of simple filtering techniques for disentangling signal and noise where needed. We argue that a cortical realization of PAL (or a variant) would be evolutionarily more advantageous than fixed feedback weights, as it implements a significantly more efficient solution to the weight transport problem. PAL requires top-down weight learning to be faster than bottom-up learning, such that error signals are transported correctly before they are used. In cortex, this could potentially be regulated by the neurotransmitter acetylcholine (ACh), involved in bottom-up and top-down attention modulation [45–47]. Learning of top-down before bottom-up weights could be modulated through release of ACh in top-down information integration sites of neurons.

Our simulation results show that PAL is able to outperform FA in terms of credit assignment in biologically plausible, recurrently connected networks. The requirements for PAL are quite general, and we stress that the dendritic microcircuit model with PAL is only one possible implementation, which however is notable for its bio-plausible error transport. In principle, it can be argued that a test error comparable to PAL could have been achieved with fixed random backprojections by scaling up the hidden layer size (not shown). Nevertheless, it is advantageous for a method to perform well while requiring fewer neurons/synapses, for biological plausibility but also energy efficiency. It has been suggested that the inefficiency of FA can be mitigated through DFA, for which we however do not find evidence. Additionally, in the context of cortical hierarchies, this presupposes skip connections from one higher cortical area to all lower areas instead of layer-wise connections. While such connections have been observed in the cortex, the visual stream is largely organized in hierarchical manner, with significantly weaker correlation between non-neighboring areas [13].

However, like any algorithm based on learning from data samples, weights trained with PAL are data-specific. That is, top-down weights are aligned with an average over many input samples \mathbf{r}_0 as $\mathbf{B}_{\ell, \ell+1} \propto \mathbb{E}[\varphi'[\mathbf{W}_{\ell+1, \ell}]^T \varphi']_{\mathbf{r}_0}$, leading to imperfect alignment of transported errors with those of backpropagation (see Fig. 3; in practice, weight alignment is restricted to at least 20°). Lower learning rates η^{bw} lead to an inclusion of more samples into the expectation value; by sampling over the whole training set, data-dependency can be minimized – however, as forward weights need to evolve slower than backward weights, this leads to slow overall learning. In contrast to this, [21] circumvents this issue by separate phases of forward and backward learning for each data sample, but no fully on-line solution is currently known. As we have shown, the error transported by this data-specific weights can still be efficient in learning to solve complex tasks.

Note that PAL is able to make full use of prospective coding – i.e., that all information propagation occurs through prospective rates $\varphi(\tilde{\mathbf{u}}_\ell)$, which converge to their steady state quasi-instantaneously. This ensures that weight updates are constructed from useful learning signals at all times, not only after the neuronal dynamics have settled into a steady state. As a consequence, we were able to simulate our dynamical system with fully continuous voltage dynamics and learning of all synapses enabled at all times. This is an important difference compared to previously known bio-plausible mechanisms of learning in dynamical systems, which have mitigated the issue of slow relaxation through slow or phased learning (see e.g. [6, 8, 26, 28–32]), and/or by re-initializing the somatic potentials to their bottom-up input state for every data sample [6, 8, 25].

As our theory is based on a rate-based abstraction of neural dynamics, there remain several open questions of bio-plausibility and realism. Extensions to our theory may implement Dale’s law of either inhibitory or excitatory activity, a constraint which could be realized by separate populations of neurons [48]. Equally, the dendritic microcircuit model could model biology more closely by implementing spiking neuronal output, and arguing that credit is assigned through a probabilistic interpretation. Future work will investigate how PAL can be related to theories of spike-based symmetrization [49].

Our results clearly point towards future work on theories of on-line learning in the cortex and on neuro-inspired hardware. Building on similar ideas in the literature [50–55], we hypothesize a general principle of using noise in physical systems for learning, instead of considering it an undesirable side effect when modeling substrates. PAL can serve as a blueprint for the greater philosophy of viewing noise as a resource rather than a nuisance.

4 Methods

As in the main text, bold lowercase (uppercase) variables \mathbf{x} (\mathbf{X}) denote vectors (matrices). The partial derivative of the activation given by $\mathbf{r}_\ell = \varphi(\check{\mathbf{u}})$ is denoted by $\varphi'(\check{\mathbf{u}})$, which is a diagonal matrix with μ -th entry $\frac{\partial r_\mu}{\partial \check{u}_\mu}$.

4.1 Prospective Coding

As neurons in our theory are modelled by leaky integrators, the somatic voltage follows the low-pass filtered sum of input currents, and therefore exhibits a slow response to its input. This effect multiplies with increasing layer number, resulting in the requirement to present an input for many membrane time constants to allow both input signals from the bottom and learning signals from the top to fully propagate through the whole network. Additionally, slow neuron dynamics do not only slow down the flow of information, but also introduce incorrect error signals, as demonstrated in Ref. [9].

Several schemes have been proposed to solve this issue. A common fix is scheduled plasticity, where synapses are only learned once the system has settled into the equilibrium state [6, 8, 26, 28–32]. This leads to slow learning, and the need to explain the phased plasticity through a biologically plausible mechanism. In Ref. [9] and our model however, the issues caused by response lag are overcome by calculating the firing rate of each neuron based on the prospective future voltage: all neural outputs and weight updates are calculated from the prospective voltage $\check{\mathbf{u}} := \mathbf{u} + \tau^{\text{eff}} \frac{d\mathbf{u}}{dt}$. The inclusion of the temporal derivative adds ‘*what neurons guess that they will be doing in the future*’ [9] to their current state. Note that the effect of prospectivity (where the output of a neuron is a function also of $\dot{\mathbf{u}}$) can already be observed in standard neuron models [56], and has been seen experimentally in Layer 5 pyramidal cells [57]; for a comprehensive explanation of biological plausibility, see Sec. 3 of Ref. [9].

The implementation of prospective coding with PAL is essential for fast transfer of information, ensuring quick convergence of weights. Noisy rates are calculated from the prospective voltage, and therefore the time delay between the top-down noise signal and the post-synaptic noise sample can become arbitrarily small. This means that the correlation time scale of the Ornstein-Uhlenbeck noise τ_ξ can also be small, leading to fast convergence of backprojections (the exact requirement on the time scales is $\tau_\xi \gtrsim \Delta t$). In comparison, methods without prospective coding require $\tau_\xi \gg \tau^{\text{eff}}$, such that top-down weights converge slowly (e.g. Ref. [25]), see Fig. 3 in Supplementary Information.

4.2 Alignment of feedback weights

We show how the weight transport problem can be solved through alignment of top-down weights. We keep our description general by discussing the basic leaky integrator model with noise,

$$\tau^{\text{eff}} \dot{\mathbf{u}}_\ell = -\mathbf{u}_\ell + \mathbf{b}_\ell + \mathbf{W}_{\ell, \ell-1} \mathbf{r}_{\ell-1} + \mathbf{e}_\ell + \boldsymbol{\xi}_\ell \quad (4)$$

with \mathbf{e}_ℓ propagated downwards from the upper layer error through feedback connections $\mathbf{B}_{\ell, \ell+1}$. As detailed in Sec. 2.1, we do not discuss error propagation itself, but focus instead on the learning of feedback weights from the rates generated within each layer. The procedure to learn the backwards weights relies on two recent theoretical advancements: the local difference reconstruction loss defined in Ref. [21] trains backwards weights to approximate backpropagation, whereas the proposal of Ref. [25] to consider Ornstein-Uhlenbeck noise enables us to learn all backwards weights simultaneously.

Concretely, for each hidden layer we sample Ornstein-Uhlenbeck noise ξ_ℓ with zero mean and a small amplitude compared to the somatic potential \mathbf{u}_ℓ . This type of noise is a natural choice to describe noisy synaptic currents, as it models synapse dynamics with Poisson input and finite (non-zero) synaptic decay times [58]. The noise term is added as a current to the soma of each hidden layer neuron, where it adds to the data signal to form a noisy firing rate. The noise changes faster than the data signals (i.e., stimulus and learning signal). This condition, $T_{\text{pres}} \gg \tau_\xi$, ensures that data and noise are separable in frequencies.

The variance of this noise can be modulated by the interplay between background firing rates and synaptic weights, while conserving its mean [59], and is often used in the diffusion approximation for stochastic neurons [60]. We note that a further interesting component is added when considering conductance-based synaptic interactions. Here, the stochasticity of neuronal membranes can depend non-monotonically on presynaptic rates, and counterintuitively decrease when rates increase [61]. A similar effect can be derived in the context of Bayesian inference [62] and has been observed experimentally [63].

To begin, we model Ornstein-Uhlenbeck noise ξ_k in each hidden layer. The noise signal is generated from low-pass filtered white noise,

$$\dot{\xi}_\ell(t) = -\frac{1}{\tau_\xi} [\xi_\ell(t) - \mu_\ell(t)], \quad (5)$$

with $\mu_\ell(t) \sim \mathcal{N}(0, \sigma^2)$, and low-pass filtering constant τ_ξ smaller than the usual presentation time T_{pres} of input signals \mathbf{r}_0 . Therefore, ξ_k represents an Ornstein-Uhlenbeck process with high frequency compared to the inference and error signals. We choose the scale of noise σ such that it is small compared to the somatic potential in all hidden layers. If we denote as $\varphi(\check{\mathbf{u}}_k^0)$ the neuron output in absence of noise, we can expand to first order in small noise, $\mathbf{r}_k \approx \varphi(\check{\mathbf{u}}_k^0) + \varphi'(\check{\mathbf{u}}_k^0) \xi_k$. This signal is sent to the corresponding higher layer $k + 1$ through the weight $\mathbf{W}_{k+1,k}$, where the upper layer noise ξ_{k+1} is added on top. This continues through all layers up to the output layer. Hence, for a given layer $\ell + 1$, the output rate is modified by noise to be

$$\mathbf{r}_{\ell+1} \approx \varphi(\check{\mathbf{u}}_{\ell+1}^0) + \varphi'(\check{\mathbf{u}}_{\ell+1}^0) \xi_{\ell+1} + \varphi'(\check{\mathbf{u}}_{\ell+1}^0) \sum_{m=1}^{\ell} \left[\prod_{n=m}^{\ell} \mathbf{W}_{n+1,n} \varphi'(\check{\mathbf{u}}_n^0) \right] \xi_m. \quad (6)$$

Note that we omit noise originating in downstream areas ($\xi_{\ell+2}, \dots, \xi_N$) as it quickly averages to zero (see below). The noise-inclusive rate $\mathbf{r}_{\ell+1}$ is also propagated top-down. In the case of layer-wise feedback connections, $\mathbf{r}_{\ell+1}$ is sent to layer ℓ through the synapse $\mathbf{B}_{\ell,\ell+1}$. Therefore, the information locally available to learn useful top-down weights is restricted to the pre-synaptic rate $\mathbf{r}_{\ell+1}$ and the post-synaptic potential including noise.

We aim now to learn the top-down synapses by exploiting the auto-correlation of noise. The slow portion $\varphi(\check{\mathbf{u}}_{\ell+1}^0)$ of the pre-synaptic signal is not useful for learning of backwards weights, as it contains correlations across layers which cannot be canceled. Therefore, we extract the noise-induced portion of the signal with a high-pass filtered version of the top-down rate, $\hat{\mathbf{r}}_{\ell+1}$ [25]. The dynamics of $\mathbf{B}_{\ell,\ell+1}$ are derived from gradient descent on the local alignment loss $\mathcal{L}_\ell^{\text{PAL}}$, defined as

$$\mathcal{L}_\ell^{\text{PAL}} = -\xi_\ell^T(t) [\mathbf{B}_{\ell,\ell+1} \hat{\mathbf{r}}_{\ell+1}(t)] + \frac{\alpha}{2} \|\mathbf{B}_{\ell,\ell+1}\|^2. \quad (7)$$

Gradient descent yields the learning rule

$$\dot{\mathbf{B}}_{\ell,\ell+1} := -\eta_\ell^{\text{bw}} \nabla_{\mathbf{B}_{\ell,\ell+1}} \mathcal{L}_\ell^{\text{PAL}} = \eta_\ell^{\text{bw}} [\xi_\ell (\hat{\mathbf{r}}_{\ell+1})^T - \alpha \mathbf{B}_{\ell,\ell+1}] \quad (8)$$

We determine the fixed point of the feedback weights by taking the expectation value over many noise samples for fixed inputs and weights,

$$0 \stackrel{!}{=} \mathbb{E}[\dot{\mathbf{B}}_{\ell, \ell+1}]_{\boldsymbol{\xi}} \quad (9)$$

$$= \mathbb{E}\left[\eta_{\ell}^{\text{bw}} \{\boldsymbol{\xi}_{\ell} (\hat{\mathbf{r}}_{\ell+1})^T - \alpha \mathbf{B}_{\ell, \ell+1}\}\right]_{\boldsymbol{\xi}} \quad (10)$$

$$\Rightarrow \mathbb{E}[\mathbf{B}_{\ell, \ell+1}]_{\boldsymbol{\xi}} = \frac{1}{\alpha} \mathbb{E}[\boldsymbol{\xi}_{\ell} (\hat{\mathbf{r}}_{\ell+1})^T]_{\boldsymbol{\xi}} \quad (11)$$

Using Eq. (6), the right hand side can be expanded,

$$\mathbb{E}[\mathbf{B}_{\ell, \ell+1}]_{\boldsymbol{\xi}} \approx \frac{1}{\alpha} \mathbb{E}\left[\boldsymbol{\xi}_{\ell} \left\{ \varphi'(\check{\mathbf{u}}_{\ell+1}^0) \boldsymbol{\xi}_{\ell+1} + \varphi'(\check{\mathbf{u}}_{\ell+1}^0) \sum_{m=1}^{\ell} \left[\prod_{n=m}^{\ell} \mathbf{W}_{n+1, n} \varphi'(\check{\mathbf{u}}_n^0) \right] \boldsymbol{\xi}_m \right\}^T\right]_{\boldsymbol{\xi}} \quad (12)$$

We now make use of the fact that the auto-covariance of Ornstein-Uhlenbeck noise decays exponentially in time,

$$\mathbb{E}[\boldsymbol{\xi}_{\ell}(t + \Delta t) \boldsymbol{\xi}_k(t)^T]_{\boldsymbol{\xi}} = \mathbf{1} \delta_{k, \ell} \frac{\sigma^2}{2} e^{-|\Delta t|/\tau_{\boldsymbol{\xi}}}, \quad (13)$$

where $\delta_{k, \ell}$ is the Kronecker delta, σ^2 the variance, and Δt corresponds to the time needed for a noise sample to travel to the layer above and back. As noise originating in different layers is uncorrelated, it quickly averages to zero, whereas the correlation of noise samples at different times generated at the same layer is non-zero. Note that PAL is compatible with different kinds of noise other than the Ornstein-Uhlenbeck type. We only require the noise to have non-zero auto-correlation time, and noise from different sources (neurons) to show vanishing correlation. This is also fulfilled e.g. by pink noise, which is ubiquitous in biological systems [64] – however, we argue that Ornstein-Uhlenbeck is a more natural model for noise in neurons due to the combination of stochastic inputs and synapses with slow dynamics. Concretely, Refs. [58, 59] have shown that neurons with Poisson spike input and a membrane acting as a low-pass filter generate Ornstein-Uhlenbeck voltage dynamics.

We thus have as our final result

$$\mathbb{E}[\mathbf{B}_{\ell, \ell+1}]_{\boldsymbol{\xi}} \approx \frac{1}{\alpha} \frac{\sigma^2}{2} e^{-|\Delta t|/\tau_{\boldsymbol{\xi}}} \left\{ \varphi'(\check{\mathbf{u}}_{\ell}^0) [\mathbf{W}_{\ell+1, \ell}]^T \varphi'(\check{\mathbf{u}}_{\ell+1}^0) \right\}. \quad (14)$$

The curly brackets show the alignment between feedback and feedforward weights.

We now incorporate this result with the learning rule for bottom-up weights $\mathbf{W}_{\ell, \ell-1}$. As discussed in Sec. 2.1, error propagation mechanisms generally produce a layer-wise error \mathbf{e}_{ℓ} as a function of top-down synapses $\mathbf{B}_{\ell, \ell+1}$.

Models closely related to backpropagation [6, 9, 31] employ forward weight updates of the form

$$\begin{aligned} \dot{\mathbf{W}}_{\ell, \ell-1} &= \eta_{\ell}^{\text{fw}} \mathbf{e}_{\ell} \mathbf{r}_{\ell-1}^T \\ &= \eta_{\ell}^{\text{fw}} \left\{ \varphi'(\check{\mathbf{u}}_{\ell}^0) \mathbf{B}_{\ell, \ell+1} \mathbf{e}_{\ell+1} \right\} \mathbf{r}_{\ell-1}^T, \end{aligned} \quad (15)$$

which applies to the model used to simulate Fig. 5 (Efficient credit assignment in deep networks). On the other hand, models where rates are propagated top-down [8, 23, 24] can be generally described by

$$\dot{\mathbf{W}}_{\ell, \ell-1} = \eta_{\ell}^{\text{fw}} \left\{ \mathbf{B}_{\ell, \ell+1} \varphi'(\check{\mathbf{u}}_{\ell+1}^0) \mathbf{e}_{\ell+1} \right\} \mathbf{r}_{\ell-1}^T; \quad (16)$$

e.g., the microcircuit model used in this work approximates this rule. We plug our result for learned top-down weights, Eq. (14), into these update rules. Because we have based our derivation on a general leaky-integrator model, our result in the form of $\mathbb{E}[\mathbf{B}_{\ell,\ell+1}] \propto \varphi'(\check{\mathbf{u}}_\ell^0) [\mathbf{W}_{\ell+1,\ell}]^T \varphi'(\check{\mathbf{u}}_{\ell+1}^0) \forall \ell$ can be employed in any of these theories. Plugging into either Eq. (15) or (16), we see that the weight updates $\Delta \mathbf{W}_{\ell,\ell-1}$ align with those of a feed-forward network trained with backpropagation up to additional factors of derivatives. Therefore, our algorithm can provide useful error signals which approximately align with backpropagation, improving on random feedback weights.

Note that PAL is also able to learn useful backprojections in absence of a teaching signal, facilitating efficient learning once an instructive signal is (re-)introduced. In particular, top-down weights do not decay to zero if forward weights are kept fixed, even though the weight decay term $\dot{\mathbf{B}}_{\ell,\ell+1} \propto -\alpha \mathbf{B}_{\ell,\ell+1}$ might suggest so. The reason for this is that the expectation value of top-down weights, Eq. (14), are formed from a balance between noise and the contribution due to the regularizer.

4.3 Dendritic cortical microcircuits

We now describe learning through minimization of the dendritic error as proposed in Ref. [8]. In this model, weights are adapted using local dendritic plasticity rules in the form $\dot{\mathbf{W}} = \eta [\varphi(\mathbf{u}) - \varphi(\mathbf{v})] \mathbf{r}^T$, where \mathbf{W} represents lateral or feed-forward weights, η is a learning rate, \mathbf{u} and \mathbf{v} denote different compartmental voltages and \mathbf{r} the pre-synaptic rate [65, 66]. In order to adhere to the principle of bio-plausibility, the microcircuit model uses rules such that \mathbf{u} corresponds to the soma of a given neuron and \mathbf{v} to the corresponding compartment the synapse connects to. The concrete form of all learning rules can be found in Supplementary Information. They are designed such that the system settles in a specific state, where activity of the apical dendrite of hidden layer pyramidal cells represents an error useful for learning.

In absence of a teaching signal, pyramidal cells take the role of representation units, reflecting feed-forward activation. They receive bottom-up information onto their basal dendrites and top-down activity in the distal apical dendrite, integrating both signals in the soma in accordance with observations of layer 2/3 pyramidal cells [67]. Pyramidal cells are described by a simplified three-compartment model with distinct basal, apical and somatic voltages [68, 69].

The interneurons in this model are present in the hidden layers, and aim to represent a copy of the activation of pyramidal cells in the layer above. Across layers, populations of pyramidal neurons and interneurons are arranged such that the number of interneurons in the hidden layers matches that of pyramidal cells in the layer above. Interneurons are modeled with two compartments, representing dendritic tree and soma. They receive lateral input from pyramidal cells in the same layer, and project back laterally to the same neurons.

We denote quantities related to pyramidal cells with upper indices ^P, while ^I marks interneurons. The dynamics of the somatic membrane potentials of pyramidal cells \mathbf{u}_ℓ^P with $\ell = 1, \dots, N-1$ are an instance of the general leaky-integrator equation (1),

$$C_m \dot{\mathbf{u}}_\ell^P = g_l (\mathbf{E}_l - \mathbf{u}_\ell^P) + g^{\text{bas}} (\mathbf{v}_\ell^{\text{bas}} - \mathbf{u}_\ell^P) + g^{\text{api}} (\mathbf{v}_\ell^{\text{api}} + \boldsymbol{\xi}_\ell(t) - \mathbf{u}_\ell^P), \quad (17)$$

where Ornstein-Uhlenbeck noise $\boldsymbol{\xi}_\ell$ is modeled at all hidden layers, and \mathbf{E}_l denotes the leak potential. We implement Latent Equilibrium into the microcircuit model as in Ref. [9] by replacing all rates calculated from somatic potentials with rates obtained from the prospective voltage, $\mathbf{r}_\ell^{\text{P/I}} = \varphi(\mathbf{u}_\ell^{\text{P/I}}) \mapsto \varphi(\check{\mathbf{u}}_\ell^{\text{P/I}})$. This affects all compartment potentials as well as synaptic plasticity rules.

We first describe learning using fixed random feedback connections. Before supervised training, the system is run in absence of a teaching signal with random input $\mathbf{r}_0(t)$. As demonstrated in

Ref. [8], the plasticity of $\mathbf{W}_{\ell,\ell}^{\text{IP}}$ and $\mathbf{B}_{\ell,\ell}^{\text{PI}}$ (see Fig. 2 for notation) allow the system to settle in a *self-predicting state*. This is a system state described by matching voltages between interneurons and pyramidal cells, $\mathbf{u}_{\ell}^{\text{I}} = \mathbf{u}_{\ell+1}^{\text{P}}$, together with zero apical voltages $\mathbf{v}_{\ell}^{\text{api}}$. This second condition is achieved in the hidden layers by learning lateral weights such that top-down and lateral activity cancel, i.e. $\mathbf{B}_{\ell,\ell}^{\text{PI}} \mathbf{r}_{\ell}^{\text{I}} = -\mathbf{B}_{\ell,\ell+1}^{\text{PP}} \mathbf{r}_{\ell+1}^{\text{P}}$.

We now turn on an instructive signal by clamping the apical compartment of top layer pyramidal cells to the target voltage \mathbf{u}^{tgt} . The somata of these neurons integrate the target signal with the bottom-up input and propagate it top-down to the hidden layers. In the limit of small conductances (weak nudging), the pyramidal neurons are now slightly nudged towards the target, while the interneurons in the hidden layers do not observe the teaching signal; therefore, they represent the activity which pyramidal cells in the layer above would have if there were no target. As the apical dendrite calculates the difference between top-down and lateral activity, it now encodes the error signal passed down to the hidden layers. This is how cortical microcircuits with dendritic error encoding assign credit to hidden layers neurons. In fact, the microcircuit model implements difference target propagation [23] in a dynamical system with recurrency, with $\mathbf{v}_{\ell}^{\text{api}} = \mathbf{B}_{\ell,\ell+1}^{\text{PP}} (\mathbf{r}_{\ell+1}^{\text{P}} - \mathbf{r}_{\ell}^{\text{I}})$ representing the backprojected difference target $g_{\ell}(\hat{\mathbf{h}}_{\ell+1}) - g_{\ell}(\mathbf{h}_{\ell+1})$. Note that the framework of DTP also includes the learning of top-down weights such that the system's cost is minimized according to Gauss-Newton optimization with batch size 1 [24]; this effect however is independent of the error propagation scheme and thus not relevant for this discussion.

As shown in Ref. [8], the weight updates in this model approximate those of error backpropagation in the limit of weak nudging (small top-down conductances):

$$\Delta \mathbf{W}_{\ell,\ell-1}^{\text{PP}} \propto \lambda^{N-\ell+1} \varphi'(\hat{\mathbf{v}}_{\ell}^{\text{bas}}) \left[\prod_{k=\ell}^{N-1} \mathbf{B}_{k,k+1}^{\text{PP}} \varphi'(\hat{\mathbf{v}}_{k+1}^{\text{bas}}) \right] \mathbf{e}_N (\mathbf{r}_{\ell-1}^{\text{P}})^T, \quad (18)$$

where $\hat{\mathbf{v}}_{\ell}^{\text{bas}} := \frac{g^{\text{bas}}}{g_1 + g^{\text{bas}} + g^{\text{api}}} \mathbf{v}_{\ell}^{\text{bas}}$ denotes the conductance-weighted feed-forward input to each pyramidal cell, $\mathbf{e}_N := \mathbf{u}^{\text{tgt}} - \hat{\mathbf{v}}_N^{\text{bas}}$ the output layer error, and a small parameter λ , which regulates the amount of top-down nudging.

PAL is implemented naturally by the inclusion of noise and our learning rule (2). Contrary to simulations with fixed top-down weights [8, 9], the inclusion of PAL also requires dynamical lateral weights from interneurons to pyramidal cells. For efficient learning, a tight balance between learning rates needs to be kept: lateral weights $\mathbf{W}_{\ell,\ell}^{\text{IP}}$ need to adapt quickly to any changes of feed-forward weights $\mathbf{W}_{\ell+1,\ell}^{\text{PP}}$, while top-down weights $\mathbf{B}_{\ell,\ell+1}^{\text{PP}}$ need to adapt to changing forward weights quickly; on the other hand, lateral weights $\mathbf{B}_{\ell,\ell}^{\text{PI}}$ from interneurons to pyramidal cells need to adapt quickly to changing top-down weights, such that no spurious error occurs. The precise order of weights updates is $|\Delta \mathbf{W}_{\ell+1,\ell}^{\text{PP}}| < |\Delta \mathbf{B}_{\ell,\ell+1}^{\text{PP}}| < |\Delta \mathbf{B}_{\ell,\ell}^{\text{PI}}| \lesssim |\Delta \mathbf{W}_{\ell,\ell}^{\text{IP}}|$.

We comment on the ability of cortical microcircuits to assign credit over hierarchies with multiple hidden layers. While Eq. 18 implies that in theory, tasks can be learned successfully using many hidden layers, the derivation assumes perfect cancellation of the top-down signal with the interneuron activity, such that only the error signal is encoded in the apical dendrite. This requires a perfect self-predicting state, which is unattainable in practice unless learning is phased (learning phases interleaved with phases where no target is present and the self-predicting state is reestablished). As the error signal scales with the small nudging strength λ , early layers in the network receive instructive signals which are weaker by orders of magnitude, further complicating realistic evaluations of the model. For this reason, we restrict our simulations showing credit assignment in cortical microcircuits to a single hidden layer (see Sections 2.3.2 & 2.3.3). We stress that this is a caveat of the microcircuit model, and not of PAL – see our results in credit assignment in deep networks, Sec. 2.3.4.

4.4 Simulation details

We stress that all simulations are performed with fully recurrent dynamics described by Eqs. (1) and (17), differentiating our work from similar studies where the dynamics are replaced by steady-state approximations and the recurrency is implicitly removed by calculating separate forward and backward passes [8, 43]. All simulation parameters are given in Supplementary Information.

In all experiments, dynamics are simulated in discrete time steps of length dt using the Euler-Maruyama method [70]. Input and targets are passed as data streams in the form of vectors presented for $T_{\text{pres}} = 100 dt$ without any kind of filtering or pre-processing. In all simulations, voltage and weight updates (where non-zero) are applied at all time steps. All layers are fully connected throughout all experiments.

Microcircuits are simulated by defining effective voltages \mathbf{u}_{eff} as described in Ref. [9]: we rewrite all dynamical equations in the form $C_m \dot{\mathbf{u}} = \frac{1}{\tau_{\text{eff}}}(\mathbf{u}_{\text{eff}} - \mathbf{u})$, where \mathbf{u} denotes the pyramidal or interneuron somatic potential. Models are initialized in the self-predicting state defined (see Supplement, and Ref. [8]). Before training, we allow the voltages to equilibrate during a brief settling phase (several dt). Activation functions are the same throughout all layers, including the output layer. Targets are provided as a target voltage \mathbf{u}^{tgt} at the output layer.

For the PAL implementations, we calculate Ornstein-Uhlenbeck noise by sampling white noise $\mathbf{w} \sim \mathcal{N}(0, 1)$ and low-pass filtering with time constant τ_ξ , that is, $\boldsymbol{\xi}_\ell[t + dt] = \boldsymbol{\xi}_\ell[t] + \frac{1}{\tau_\xi}(\sqrt{\tau_\xi dt} \sigma_\ell \mathbf{w} - dt \boldsymbol{\xi}_\ell[t])$. High-pass filtered rates $\hat{\mathbf{r}}_\ell$ are calculated with respect to the time constant τ_{hp} through $\frac{d\hat{\mathbf{r}}_\ell^{\text{P}}}{dt} = \frac{d\mathbf{r}_\ell^{\text{P}}}{dt} - \frac{\hat{\mathbf{r}}_\ell^{\text{P}}}{\tau_{\text{hp}}}$. Forward weight updates low-pass filtered with τ_{lo} before application.

For pseudocode, all parameters and architecture details, see Supplementary Information. Due to the intricate interplay of parameters specific to PAL ($\eta^{\text{bw}}, \sigma_\ell, \alpha, \tau_{\text{lo}}, \tau_{\text{hp}}, \tau_\xi$) with the large number of parameters which the dendritic microcircuit framework already carries, we restricted our parameter search to the set of all learning rates and some of the PAL parameters, $\{\eta^{\text{fw}}, \eta^{\text{bw}}, \eta^{\text{IP}}, \eta^{\text{PI}}, \sigma_\ell, \alpha, \tau_{\text{lo}}\}$. Simulations were optimized using these parameters by hand, ensuring the order of weight updates to comply without our findings of Sec. 4.3. The remaining parameters were set according to our assumptions about PAL, or, in the case of conductances, inherited from Ref. [9].

4.4.1 Phaseless backwards weight alignment

We simulate a microcircuit network of size [5-20-10-20-5] with sigmoid activation. Linear and non-linear regimes are simulated by choosing bottom-up weights as $\mathbf{W}^{\text{PP}} \sim \mathcal{U}[-1, 1]$ and $\sim \mathcal{U}[-5, 5]$, respectively. Forward weights are fixed, while top-down and lateral (inter- to pyramidal neuron) weights are learned.

During evaluation against BP (right column in Fig. 3), we set the lateral weights during to the exact self-predicting state, in order to observe an error signal in earlier hidden layers. Note that the weight updates in the microcircuit model do not exactly represent those of an ANN. This is due to an additional factor $\varphi'(\check{\mathbf{u}}_N^{\text{P}})$ as well as the fact that top-down nudging influences the somatic activity (see Supplementary Information for details). These factors introduce a misalignment unrelated to the performance of PAL, as can be seen through the comparison of updates in the non-linear case (Fig. 3 (f)); in particular, already in the output layer ($\ell = 4$), a misalignment of $\sim 20^\circ$ can be observed, and hence even perfectly learned backprojections are likely to observe increased misalignment. Therefore, it is to be expected that alignment is improved further in theories of error propagation which relate more closely to backpropagation.

In order to illustrate the advantages of prospective coding (Fig. 3), we re-ran the experiments

of Fig. 3 (a,b,c) with time constants $\{T_{\text{pres}}, \tau_{\text{hp}}, \tau_{\xi}\}$ rescaled by 10 and 100, while rescaling all learning rates by the inverse. Runs without prospective coding used the rate output $\mathbf{r}_{\ell} = \varphi(\mathbf{u}_{\ell})$ instead of $\varphi(\check{\mathbf{u}}_{\ell})$.

4.4.2 Classification experiments

The Yin-yang and MNIST tasks were solved using microcircuit networks of size [4-30-3] and [784-100-10], respectively, with sigmoid activation. All weights (including lateral) were trained with fully recurrent dynamics. For the experiments shown in this section we use the GPU enhanced Neuronal Network simulation environment (GeNN) [71, 72]. Natively, GeNN supports the simulation of spiking neural networks, but the possibility to add custom neuron and synapse models to the already provided ones makes the implementation of rate-based models such as the dendritic microcircuit possible. The simulation of the dendritic microcircuits benefited greatly from the GPU support provided by GeNN which allowed us to perform the experiments shown in this section within practically feasible simulation times.

As shown in Fig. 4 (c,d,e,f), PAL is able to outperform FA in benchmark tasks. However, this may be the case simply due to the inclusion of noise on neuronal dynamics. In order to demonstrate that top-down learning with PAL is really required for increased performance, we have simulated PAL with top-down learning turned off, which is equivalent to a network trained with FA with noise. The results are shown in Fig. 2 in Supplementary Information and show that indeed, top-down alignment facilitated by PAL is required for increased performance.

4.4.3 Efficient credit assignment in deep networks

For these experiments, we simulated the general leaky integrator model, Eq. (1). As previously, this model was simulated in discrete time steps, with images presented for $T_{\text{pres}} = 100$ dt. Voltages were updated continuously, and weight updates are applied at all steps. The output layer error was defined as $\mathbf{e}_N = \mathbf{u}^{\text{tgt}} - \check{\mathbf{u}}_N$, and hidden layer errors are calculated via $\mathbf{e}_{\ell} = \varphi' \cdot \mathbf{B}_{\ell, \ell+1}[\check{\mathbf{u}}_{\ell+1} - \mathbf{W}_{\ell+1, \ell} \mathbf{r}_{\ell}]$. We have also included a bias term for each neuron. PAL was implemented by adding Ornstein-Uhlenbeck noise ξ_{ℓ} to each hidden layer neuron, calculating the high-pass filtered rate $\hat{\mathbf{r}}_{\ell+1}$ and updating top-down weights with Eq. (2).

Network size of the autoencoder was [784-200-2-200-784], with activations [tanh, linear, tanh, linear]. We define as latent space activity the output of the two neurons in the central hidden layer. After every epoch of training the LI model, we trained a linear classifier on the MNIST train set and show the accuracy of the linear classifier on the test set.

For the CIFAR-10 experiments, we built on the continuous-time variant of LeNet-5 of Ref. [9]. In order to achieve our results on these time-consuming simulations, we have made a simplification: top-down signals (errors) are not added to the somata, such that the full soma dynamics are

$$\tau \dot{\mathbf{u}}_{\ell} = -\mathbf{u}_{\ell} + \mathbf{b}_{\ell} + \mathbf{W}_{\ell, \ell-1} \mathbf{r}_{\ell-1} + \xi_{\ell}. \quad (19)$$

This weakens the recurrency of all signals in the network, making it easier to train with all algorithms. As a consequence, error signals are passed top-down directly as $\mathbf{e}_{\ell} = \varphi' \cdot \mathbf{B}_{\ell, \ell+1} \mathbf{e}_{\ell+1}$.

The network consists of four layers: Conv2d($(5 \times 5) \times 20$) with sigmoid and MaxPool(2) activation, Conv2d($(5 \times 5) \times 50$) with sigmoid and MaxPool(2) activation, a fully-connected projection layer of 500 neurons and a linear output layer with 10 neurons. With PAL, we train the top-down weights from the second Conv2d layer to the projection layer and from the projection to the output layer, as the remaining bottom-up connection (Conv2d to Conv2d) is a kernel, for which PAL is not defined. For the second layer, noise is added after the MaxPool(2) activation instead of on top of the somata, as this increases convergence time of top-down weights. Validation

and test accuracies are determined without noise, in order to enable a fair comparison with other methods.

In these experiments, hyperparameter optimization was carried out by a grid search over η^{fw} , while the remaining parameters were optimized manually. See Tab. 2 in Supplement for parameters.

Data availability statement

The datasets analyzed during the current study are publicly available in the following repositories: https://github.com/lkriener/yin_yang_data_set (Yin-Yang dataset [42]), <http://yann.lecun.com/exdb/mnist/> (MNIST dataset [73]), <https://www.cs.toronto.edu/~kriz/cifar.html> (CIFAR-10 [74]).

Code availability

All code is made available under <https://doi.org/10.5281/zenodo.10401883>.

Acknowledgment

We wish to thank Jakob Jordan, Alexander Meulemans and João Sacramento for valuable discussions. We gratefully acknowledge funding from the European Union under grant agreements 604102, 720270, 785907, 945539 (HBP) and the Manfred Stärk Foundation. Additionally, our work has greatly benefited from access to the Fenix Infrastructure resources, which are partially funded from the European Union’s Horizon 2020 research and innovation programme through the ICEI project under the grant agreement No. 800858. This includes access to Piz Daint at the Swiss National Supercomputing Centre, Switzerland. Further calculations were performed on UBELIX, the HPC cluster at the University of Bern.

Author contributions

K.M. derived, with contributions by L.K. and M.A.P., the phaseless alignment learning (PAL) algorithm. K.M. and L.K. adapted the dendritic microcircuit model to include PAL for learning the feedback weights. G.G. and T.N. developed a dendritic microcircuit module for the GeNN simulator. L.K. added the latent equilibrium and PAL mechanisms to the module. K.M. and L.K. performed the simulation experiments. I.J. and K.M. worked on scaling the algorithm to a larger benchmark during the revision process. The manuscript was mainly written by K.M., aided by L.K. and M.A.P. M.A.P. and W.S. provided supervision and funding to this project.

Competing interests

The authors declare no competing interests.

References

- [1] D. L. K. Yamins and J. J. DiCarlo. “Using goal-driven deep learning models to understand sensory cortex”. In: *Nature Neuroscience* 19.3 (Mar. 2016), pp. 356–365.
- [2] B. A. Richards et al. “A deep learning framework for neuroscience”. In: *Nature neuroscience* 22.11 (2019), pp. 1761–1770.
- [3] T. P. Lillicrap et al. “Backpropagation and the brain”. In: *Nature Reviews Neuroscience* 21.6 (June 2020), pp. 335–346.
- [4] P. Roelfsema and A. Ooyen. “Attention-Gated Reinforcement Learning of Internal Representations for Classification”. In: *Neural computation* 17 (Nov. 1, 2005), pp. 2176–214. DOI: 10.1162/0899766054615699.
- [5] R. Costa et al. “Cortical microcircuits as gated-recurrent neural networks”. In: *Advances in neural information processing systems* 30 (2017).
- [6] B. Scellier and Y. Bengio. “Equilibrium propagation: Bridging the gap between energy-based models and backpropagation”. In: *Frontiers in computational neuroscience* 11 (2017), p. 24.
- [7] J. C. R. Whittington and R. Bogacz. “An Approximation of the Error Backpropagation Algorithm in a Predictive Coding Network with Local Hebbian Synaptic Plasticity”. In: *Neural Computation* 29.5 (May 2017), pp. 1229–1262. ISSN: 0899-7667. DOI: 10.1162/NECO_a_00949. eprint: https://direct.mit.edu/neco/article-pdf/29/5/1229/2015080/neco_a_00949.pdf. URL: https://doi.org/10.1162/NECO_a_00949.
- [8] J. Sacramento et al. “Dendritic cortical microcircuits approximate the backpropagation algorithm”. In: *Advances in neural information processing systems* 31 (2018).
- [9] P. Haider et al. “Latent Equilibrium: A unified learning theory for arbitrarily fast computation with arbitrarily slow neurons”. In: *Advances in Neural Information Processing Systems* 34 (2021), pp. 17839–17851.
- [10] T. P. Lillicrap et al. “Random synaptic feedback weights support error backpropagation for deep learning”. In: *Nature communications* 7.1 (2016), pp. 1–10.
- [11] A. Payeur et al. “Burst-dependent synaptic plasticity can coordinate learning in hierarchical circuits”. In: *Nature neuroscience* 24.7 (2021), pp. 1010–1019.
- [12] A. H. Marblestone, G. Wayne, and K. P. Kording. “Toward an Integration of Deep Learning and Neuroscience”. In: *Frontiers in Computational Neuroscience* 10 (2016), p. 94. ISSN: 1662-5188. DOI: 10.3389/fncom.2016.00094. URL: <https://www.frontiersin.org/article/10.3389/fncom.2016.00094>.
- [13] K. V. Haak and C. F. Beckmann. “Objective analysis of the topological organization of the human cortical visual connectome suggests three visual pathways”. In: *Cortex* 98 (2018), pp. 73–83. ISSN: 0010-9452. DOI: <https://doi.org/10.1016/j.cortex.2017.03.020>. URL: <https://www.sciencedirect.com/science/article/pii/S0010945217301004>.
- [14] J. Friedrich, R. Urbanczik, and W. Senn. “Spatio-temporal credit assignment in neuronal population learning”. In: *PLoS computational biology* 7.6 (June 2011), e1002092. ISSN: 1553-7358. DOI: 10.1371/journal.pcbi.1002092.
- [15] D. E. Rumelhart, G. E. Hinton, and R. J. Williams. “Learning representations by back-propagating errors”. In: *nature* 323.6088 (1986), pp. 533–536.
- [16] Y. LeCun et al. “A theoretical framework for back-propagation”. In: *Proceedings of the 1988 connectionist models summer school*. Vol. 1. 1988, pp. 21–28.

- [17] A. Nøkland. “Direct feedback alignment provides learning in deep neural networks”. In: *Advances in neural information processing systems* 29 (2016).
- [18] J. Kolen and J. Pollack. “Backpropagation without weight transport”. In: *Proceedings of 1994 IEEE International Conference on Neural Networks (ICNN’94)*. Vol. 3. 1994, 1375–1380 vol.3. DOI: 10.1109/ICNN.1994.374486.
- [19] M. Akrouf et al. “Deep learning without weight transport”. In: *arXiv preprint arXiv:1904.05391* (2019).
- [20] B. J. Lansdell, P. R. Prakash, and K. P. Kording. “Learning to solve the credit assignment problem”. In: *International Conference on Learning Representations*. 2020.
- [21] M. M. Ernoult et al. “Towards Scaling Difference Target Propagation by Learning Backprop Targets”. In: *Proceedings of the 39th International Conference on Machine Learning*. Ed. by K. Chaudhuri et al. Vol. 162. Proceedings of Machine Learning Research. PMLR, 2022, pp. 5968–5987. URL: <https://proceedings.mlr.press/v162/ernoult22a.html>.
- [22] Y. Bengio. “How auto-encoders could provide credit assignment in deep networks via target propagation”. In: *arXiv preprint arXiv:1407.7906* (2014).
- [23] D.-H. Lee et al. “Difference target propagation”. In: *Joint european conference on machine learning and knowledge discovery in databases*. Springer. 2015, pp. 498–515.
- [24] A. Meulemans et al. “A Theoretical Framework for Target Propagation”. In: *Advances in Neural Information Processing Systems*. Ed. by H. Larochelle et al. Vol. 33. Curran Associates, Inc., 2020, pp. 20024–20036. URL: <https://proceedings.neurips.cc/paper/2020/file/e7a425c6ece20cbc9056f98699b53c6f-Paper.pdf>.
- [25] A. Meulemans et al. “Credit assignment in neural networks through deep feedback control”. In: *Advances in Neural Information Processing Systems* 34 (2021).
- [26] R. C. O’Reilly. “Biologically Plausible Error-Driven Learning Using Local Activation Differences: The Generalized Recirculation Algorithm”. In: *Neural Computation* 8.5 (1996), pp. 895–938. DOI: 10.1162/neco.1996.8.5.895.
- [27] D. H. Ackley, G. E. Hinton, and T. J. Sejnowski. “A Learning Algorithm for Boltzmann Machines”. In: *Readings in Computer Vision*. Ed. by M. A. Fischler and O. Firschein. San Francisco (CA): Morgan Kaufmann, Jan. 1, 1987, pp. 522–533. ISBN: 978-0-08-051581-6. DOI: 10.1016/B978-0-08-051581-6.50053-2. URL: <https://www.sciencedirect.com/science/article/pii/B9780080515816500532> (visited on 09/27/2022).
- [28] Y. Bengio and A. Fischer. “Early inference in energy-based models approximates back-propagation”. In: *arXiv preprint arXiv:1510.02777* (2015).
- [29] J. Guerguiev, T. P. Lillicrap, and B. A. Richards. “Towards deep learning with segregated dendrites”. In: *ELife* 6 (2017), e22901.
- [30] T. Mesnard et al. “Ghost units yield biologically plausible backprop in deep neural networks”. In: *arXiv preprint arXiv:1911.08585* (2019).
- [31] X. Xie and H. S. Seung. “Equivalence of Backpropagation and Contrastive Hebbian Learning in a Layered Network”. In: *Neural Computation* 15.2 (Feb. 2003), pp. 441–454. ISSN: 0899-7667. DOI: 10.1162/089976603762552988. eprint: <https://direct.mit.edu/neco/article-pdf/15/2/441/815498/089976603762552988.pdf>. URL: <https://doi.org/10.1162/089976603762552988>.

- [32] Y. Song et al. “Inferring Neural Activity Before Plasticity: A Foundation for Learning Beyond Backpropagation”. In: *bioRxiv* (2022). DOI: 10.1101/2022.05.17.492325. eprint: <https://www.biorxiv.org/content/early/2022/05/18/2022.05.17.492325.full.pdf>. URL: <https://www.biorxiv.org/content/early/2022/05/18/2022.05.17.492325>.
- [33] I. Pozzi, S. Bohte, and P. Roelfsema. “Attention-Gated Brain Propagation: How the brain can implement reward-based error backpropagation”. In: *Advances in Neural Information Processing Systems*. Ed. by H. Larochelle et al. Vol. 33. Curran Associates, Inc., 2020, pp. 2516–2526. URL: <https://proceedings.neurips.cc/paper/2020/file/1abb1e1ea5f481b589da52303b091cbb-Paper.pdf>.
- [34] I. Pozzi, S. Bohté, and P. Roelfsema. “A biologically plausible learning rule for deep learning in the brain”. In: *arXiv preprint arXiv:1811.01768* (2018).
- [35] T. H. Moskovitz, A. Litwin-Kumar, and L. Abbott. “Feedback alignment in deep convolutional networks”. In: *arXiv preprint arXiv:1812.06488* (2018).
- [36] S. Bartunov et al. “Assessing the scalability of biologically-motivated deep learning algorithms and architectures”. In: *arXiv preprint arXiv:1807.04587* (2018).
- [37] K. Archer, K. Pammer, and T. R. Vidyasagar. “A temporal sampling basis for visual processing in developmental dyslexia”. In: *Frontiers in Human Neuroscience* 14 (2020), p. 213.
- [38] H. Gray. *Anatomy of the Human Body*. 1918. URL: <https://commons.wikimedia.org/wiki/File:Gray728.svg>.
- [39] C. Bidoret et al. “Presynaptic NR2A-containing NMDA receptors implement a high-pass filter synaptic plasticity rule”. In: *Proceedings of the National Academy of Sciences* 106.33 (2009), pp. 14126–14131.
- [40] C. Clopath et al. “Connectivity reflects coding: a model of voltage-based STDP with homeostasis”. In: *Nature Neuroscience* 13.3 (Mar. 2010). Number: 3 Publisher: Nature Publishing Group, pp. 344–352. ISSN: 1546-1726. DOI: 10.1038/nn.2479. URL: <https://www.nature.com/articles/nn.2479> (visited on 09/26/2022).
- [41] J. Bono and C. Clopath. “Modeling somatic and dendritic spike mediated plasticity at the single neuron and network level”. In: *Nature Communications* 8.1 (Dec. 2017), p. 706. ISSN: 2041-1723. DOI: 10.1038/s41467-017-00740-z. URL: <http://www.nature.com/articles/s41467-017-00740-z> (visited on 09/23/2022).
- [42] L. Kriener, J. Göltz, and M. A. Petrovici. “The yin-yang dataset”. In: *arXiv preprint arXiv:2102.08211* (2021).
- [43] W. Greedy et al. “Single-phase deep learning in cortico-cortical networks”. In: *Advances in Neural Information Processing Systems*. Ed. by S. Koyejo et al. Vol. 35. Curran Associates, Inc., 2022, pp. 24213–24225.
- [44] B. Crafton et al. “Direct feedback alignment with sparse connections for local learning”. In: *Frontiers in neuroscience* 13 (2019), p. 525.
- [45] H. Sato et al. “A functional role of cholinergic innervation to neurons in the cat visual cortex”. In: *Journal of neurophysiology* 58.4 (1987), pp. 765–780.
- [46] S. Soma et al. “Cholinergic modulation of response gain in the primary visual cortex of the macaque”. In: *Journal of neurophysiology* 107.1 (2012), pp. 283–291.
- [47] J. I. Kang, F. Huppé-Gourgues, and E. Vaucher. “Boosting visual cortex function and plasticity with acetylcholine to enhance visual perception”. In: *Frontiers in systems neuroscience* (2014), p. 172.

- [48] J. Cornford et al. “Learning to live with Dale’s principle: ANNs with separate excitatory and inhibitory units”. In: *bioRxiv* (2021). DOI: 10.1101/2020.11.02.364968. eprint: <https://www.biorxiv.org/content/early/2021/04/02/2020.11.02.364968.full.pdf>. URL: <https://www.biorxiv.org/content/early/2021/04/02/2020.11.02.364968>.
- [49] K. S. Burbank. “Mirrored STDP implements autoencoder learning in a network of spiking neurons”. In: *PLoS computational biology* 11.12 (2015), e1004566.
- [50] W. Maass. “Noise as a Resource for Computation and Learning in Networks of Spiking Neurons”. In: *Proceedings of the IEEE* 102.5 (2014), pp. 860–880. DOI: 10.1109/JPROC.2014.2310593.
- [51] D. A. Rusakov, L. P. Savtchenko, and P. E. Latham. “Noisy Synaptic Conductance: Bug or a Feature?” In: *Trends in Neurosciences* 43.6 (2020), pp. 363–372. ISSN: 0166-2236. DOI: 10.1016/j.tins.2020.03.009. URL: <https://doi.org/10.1016/j.tins.2020.03.009>.
- [52] M. D. McDonnell and L. M. Ward. “The benefits of noise in neural systems: bridging theory and experiment”. In: *Nature Reviews Neuroscience* 12.7 (2011), pp. 415–425. ISSN: 1471-0048. DOI: 10.1038/nrn3061. URL: <https://doi.org/10.1038/nrn3061>.
- [53] A. A. Faisal, L. P. J. Selen, and D. M. Wolpert. “Noise in the nervous system”. In: *Nature Reviews Neuroscience* 9.4 (2008), pp. 292–303. ISSN: 1471-0048. DOI: 10.1038/nrn2258. URL: <https://doi.org/10.1038/nrn2258>.
- [54] X. Xie and H. S. Seung. “Learning in neural networks by reinforcement of irregular spiking”. In: *Physical Review E* 69.4 (Apr. 30, 2004). Publisher: American Physical Society, p. 041909. DOI: 10.1103/PhysRevE.69.041909. URL: <https://link.aps.org/doi/10.1103/PhysRevE.69.041909> (visited on 06/30/2023).
- [55] I. R. Fiete, M. S. Fee, and H. S. Seung. “Model of birdsong learning based on gradient estimation by dynamic perturbation of neural conductances”. In: *Journal of neurophysiology* 98.4 (2007), pp. 2038–2057.
- [56] H. E. Plesser and W. Gerstner. “Escape rate models for noisy integrate-and-free neurons”. In: *Neurocomputing* 32 (2000), pp. 219–224.
- [57] H. Köndgen et al. “The Dynamical Response Properties of Neocortical Neurons to Temporally Modulated Noisy Inputs In Vitro”. In: *Cerebral Cortex* 18.9 (Feb. 2008), pp. 2086–2097. ISSN: 1047-3211. DOI: 10.1093/cercor/bhm235. eprint: <https://academic.oup.com/cercor/article-pdf/18/9/2086/17299890/bhm235.pdf>. URL: <https://doi.org/10.1093/cercor/bhm235>.
- [58] M. A. Petrovici et al. “Stochastic inference with spiking neurons in the high-conductance state”. In: *Physical Review E* 94.4 (2016), p. 042312.
- [59] L. M. Ricciardi and L. Sacerdote. “The Ornstein-Uhlenbeck process as a model for neuronal activity: I. Mean and variance of the firing time”. In: *Biological cybernetics* 35.1 (1979), pp. 1–9.
- [60] W. Gerstner et al. *Neuronal dynamics: From single neurons to networks and models of cognition*. Cambridge University Press, 2014.
- [61] M. A. Petrovici. *Form versus function: theory and models for neuronal substrates*. Vol. 1. Springer, 2016.
- [62] J. Jordan et al. “Learning Bayes-optimal dendritic opinion pooling”. In: *arXiv preprint arXiv:2104.13238* (2021).
- [63] S. Crochet et al. “Synaptic mechanisms underlying sparse coding of active touch”. In: *Neuron* 69.6 (2011), pp. 1160–1175.

- [64] P Szendro, G. Vincze, and A Szasz. “Bio-response to white noise excitation”. In: *Electro-and Magnetobiology* 20.2 (2001), pp. 215–229.
- [65] R. Urbanczik and W. Senn. “Learning by the Dendritic Prediction of Somatic Spiking”. In: *Neuron* 81.3 (2014), pp. 521–528. ISSN: 0896-6273. DOI: <https://doi.org/10.1016/j.neuron.2013.11.030>. URL: <https://www.sciencedirect.com/science/article/pii/S0896627313011276>.
- [66] W. Gerstner et al. “Eligibility Traces and Plasticity on Behavioral Time Scales: Experimental Support of NeoHebbian Three-Factor Learning Rules”. In: *Frontiers in Neural Circuits* 12 (2018). ISSN: 1662-5110. DOI: 10.3389/fncir.2018.00053. URL: <https://www.frontiersin.org/articles/10.3389/fncir.2018.00053>.
- [67] R. Jordan and G. B. Keller. “Opposing influence of top-down and bottom-up input on excitatory layer 2/3 neurons in mouse primary visual cortex”. In: *Neuron* 108.6 (2020), pp. 1194–1206.
- [68] K. P. Körding and P. König. “Supervised and Unsupervised Learning with Two Sites of Synaptic Integration”. In: *Journal of Computational Neuroscience* 11.3 (Nov. 1, 2001), pp. 207–215. ISSN: 1573-6873. DOI: 10.1023/A:1013776130161. URL: <https://doi.org/10.1023/A:1013776130161> (visited on 09/23/2022).
- [69] N. Spruston. “Pyramidal neurons: dendritic structure and synaptic integration”. In: *Nature Reviews Neuroscience* 9.3 (Mar. 2008). Number: 3 Publisher: Nature Publishing Group, pp. 206–221. ISSN: 1471-0048. DOI: 10.1038/nrn2286. URL: <https://www.nature.com/articles/nrn2286> (visited on 09/27/2022).
- [70] S. Särkkä and A. Solin. *Applied Stochastic Differential Equations*. Institute of Mathematical Statistics Textbooks. Cambridge University Press, 2019. DOI: 10.1017/9781108186735.
- [71] E. Yavuz, J. Turner, and T. Nowotny. “GeNN: a code generation framework for accelerated brain simulations”. In: *Scientific reports* 6.1 (2016), pp. 1–14.
- [72] J. C. Knight, A. Komissarov, and T. Nowotny. “PyGeNN: a Python library for GPU-enhanced neural networks”. In: *Frontiers in Neuroinformatics* 15 (2021), p. 659005.
- [73] Y. LeCun et al. “Gradient-based learning applied to document recognition”. In: *Proceedings of the IEEE* 86.11 (1998), pp. 2278–2324.
- [74] A. Krizhevsky, G. Hinton, et al. “Learning multiple layers of features from tiny images”. In: (2009).
- [75] B. Podlaski and C. K. Machens. “Biological credit assignment through dynamic inversion of feedforward networks”. In: *Advances in Neural Information Processing Systems*. Ed. by H. Larochelle et al. Vol. 33. Curran Associates, Inc., 2020, pp. 10065–10076. URL: <https://proceedings.neurips.cc/paper/2020/file/7261925973c9bf0a74d85ae968a57e5f-Paper.pdf>.

A Additional information on PAL

In this Supplement, we give more detail on the derivation and application of PAL (App. A.1) and the microcircuit implementation (App. A.2) used to perform the simulations.

As in the main text, bold lowercase (uppercase) variables \mathbf{x} (\mathbf{X}) denote vectors (matrices). The partial derivative of the activation given by $\mathbf{r}_\ell = \varphi(\check{\mathbf{u}})$ is denoted by $\varphi'(\check{\mathbf{u}})$, which is a diagonal matrix with μ -th entry $\frac{\partial r_\mu}{\partial \check{u}_\mu}$.

A.1 Derivation of PAL

We point out how and why our alignment loss $\mathcal{L}_\ell^{\text{PAL}}$, defined in Eq. (7), differs from the reconstruction loss $\widehat{\mathcal{L}}$ introduced in Ref. [21]. Using the notation of this manuscript, this can be expressed as

$$\widehat{\mathcal{L}}_{\mathbf{B}_{\ell,\ell+1}}^\ell \cong -\boldsymbol{\xi}_\ell^T \mathbf{B}_{\ell,\ell+1} \{ \mathbf{r}_{\ell+1}^{\boldsymbol{\xi}_\ell} - \varphi(\check{\mathbf{u}}_{\ell+1}^0) \} + \left\| \mathbf{B}_{\ell,\ell+1} \{ \mathbf{r}_{\ell+1}^{\boldsymbol{\xi}_{\ell+1}} - \varphi(\check{\mathbf{u}}_{\ell+1}^0) \} \right\|^2, \quad (20)$$

where $\mathbf{r}_{\ell+1}^{\boldsymbol{\xi}_\ell}$ is the rate which comprising data signal and noise from layer ℓ only, while the second term generated from $\check{\mathbf{u}}_\ell^0$ contains no noise signal. The regularizer requires a separate phase, where noise is injected only into layer $\ell + 1$ and backpropagated to layer ℓ .

Training feedback weights by gradient descent on this alignment loss represents a case closely related to PAL – for fixed input and forward weights, $\mathbf{B}_{\ell,\ell+1}$ converges such that the Jacobians matrices align, $\mathbf{B}_{\ell,\ell+1} \varphi'(\check{\mathbf{u}}_{\ell+1}^0) \parallel [\varphi'(\check{\mathbf{u}}_\ell^0) \mathbf{W}_{\ell+1,\ell}]^T$. Inserting this result into the difference target propagation rule of Eq. (16), we see that the update reproduces exact backpropagation with linear activation function on the output layer.

An analogous implementation of gradient descent on $\widehat{\mathcal{L}}$ in our setup requires making use of the noise in the output layer, and using a different kind of regularizer, i.e. $-\alpha \|\mathbf{B}_{\ell,\ell+1} \widehat{\mathbf{r}}_{\ell+1}\|^2$ instead of weight decay. Unfortunately, this regularizer contains non-zero correlations of all noise signals up to layer $\ell + 1$, and not only auto-correlations of $\boldsymbol{\xi}_\ell$. Therefore, gradient descent on a difference reconstruction loss with this regularizer does not lead to useful top-down weights, as a particular weight $\mathbf{B}_{\ell,\ell+1}$ receives contributions proportional to all weights $\mathbf{W}_{k+1,k}$ for $k = 1 \dots \ell$. The central reason causing this issue is that our system learns to adapt all feedback weights simultaneously, which requires considering noise in all layers at all times. Contrary to this, in Ref. [21], feedback weights are trained sequentially with two separate phases of noise injections in different layers. We have therefore designed Eq. (8) as a heuristic approximation to the optimal update rule, while achieving full always-on plasticity in our system.

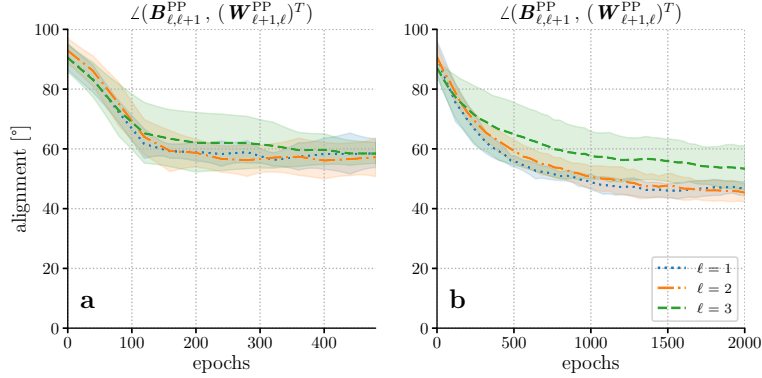
Alternatively, the problem of superfluous derivatives φ' can be addressed if the derivative of the activation w.r.t. to the potential is available at the synapse. Given this information, the weight updates can be defined as

$$\dot{\mathbf{B}}_{\ell,\ell+1} = \eta_\ell^{\text{bw}} [\boldsymbol{\xi}_\ell (\widehat{\mathbf{r}}_{\ell+1})^T - \alpha \varphi'(\check{\mathbf{u}}_\ell) \mathbf{B}_{\ell,\ell+1} \varphi'(\check{\mathbf{u}}_{\ell+1})]. \quad (21)$$

Note that the derivatives $\varphi'(\check{\mathbf{u}}_\ell)$ are a function of the full somatic potential, comprising data as well as noise. Using the fact that correlations between $\boldsymbol{\xi}_\ell$ and $\boldsymbol{\xi}_{\ell+1}$ cancel to zero, we obtain that the new expectation value of top-down weights to first order,

$$\mathbb{E}[\varphi'(\check{\mathbf{u}}_\ell^0) \mathbf{B}_{\ell,\ell+1} \varphi'(\check{\mathbf{u}}_{\ell+1}^0)]_{\boldsymbol{\xi}} \propto \varphi'(\check{\mathbf{u}}_\ell^0) [\mathbf{W}_{\ell+1,\ell}]^T \varphi'(\check{\mathbf{u}}_{\ell+1}^0). \quad (22)$$

We have tested this alternative regularizer in the relevant regime of in non-linear activation. As shown in Fig. 1, it is able to improve alignment of $\mathbf{B}_{\ell,\ell+1}^{\text{PP}}$ with $[\mathbf{W}_{\ell+1,\ell}^{\text{PP}}]^T$ by about 10° in this



Supplementary Figure 1: Alternative regularizer with derivative shows further improvement in alignment. We reproduce the experiment in Fig. 3 (e) using the same parameters: microcircuits learning to adapt backwards weights with PAL using (a) the standard weight decay regularizer and (b) the derivative-dependent regularizer of Eq. (21).

example (note that we have used the same parameters as in the PAL setup. With appropriate hyperparameter search, convergence time and final alignment may be improved). However, whether a bio-plausible synapse can calculate the derivative $\varphi' = \frac{\partial \varphi}{\partial \mathbf{u}}$ is not clear. Given our requirement that all computations can be implemented with simple physical components, we have opted for the weight decay regularizer as defined in Eq. (7).

A.2 Error propagation in microcircuits

In this section, we explain in detail how the cortical microcircuit is able to propagate meaningful targets, and align its feedback weights using PAL in order to efficiently minimize the difference between its output and a teaching signal.

We briefly review the general microcircuit setup defined by Ref. [8]. In this model, the different neuron populations are each selected to play a distinct role. Each hidden layer is composed of a population of pyramidal neurons and interneurons, where the number of interneurons in a given layer matches the number of pyramidal cells in the layer above. The neurons form a network defined by connections as shown in Fig. 2.

As in Ref. [8], we define the following coupled differential equations to govern the voltage dynamics of pyramidal cells (\mathbf{u}_ℓ^P) and interneurons (\mathbf{u}_ℓ^I) in a network with layers $\ell = 1 \dots N$:

$$C_m \dot{\mathbf{u}}_\ell^P = g_l (\mathbf{E}_1 - \mathbf{u}_\ell^P) + g^{\text{bas}} (\mathbf{v}_\ell^{\text{bas}} - \mathbf{u}_\ell^P) + g^{\text{api}} (\mathbf{v}_\ell^{\text{api}} + \boldsymbol{\xi}_\ell(t) - \mathbf{u}_\ell^P) \quad \forall \ell \neq N, \quad (23)$$

$$C_m \dot{\mathbf{u}}_N^P = g_l (\mathbf{E}_1 - \mathbf{u}_N^P) + g^{\text{bas}} (\mathbf{v}_N^{\text{bas}} - \mathbf{u}_N^P) + \mathbf{i}^{\text{nudge,tgt}}, \quad (24)$$

$$C_m \dot{\mathbf{u}}_\ell^I = g_l (\mathbf{E}_1 - \mathbf{u}_\ell^I) + g^{\text{den}} (\mathbf{v}^{\text{den}} - \mathbf{u}_\ell^I) + \mathbf{i}^{\text{nudge,I}}. \quad (25)$$

Here, $\boldsymbol{\xi}_\ell$ denotes the noise modeled in all hidden layers. Compartment voltages are induced instantaneously by the respective input rates and synaptic weight,

$$\mathbf{v}_\ell^{\text{bas}} = \mathbf{W}_{\ell,\ell-1}^{\text{PP}} \varphi(\check{\mathbf{u}}_{\ell-1}^P), \quad (26)$$

$$\mathbf{v}_\ell^{\text{api}} = \mathbf{B}_{\ell,\ell+1}^{\text{PP}} \varphi(\check{\mathbf{u}}_{\ell+1}^P) + \mathbf{B}_{\ell,\ell}^{\text{PI}} \varphi(\check{\mathbf{u}}_\ell^I), \quad (27)$$

$$\mathbf{v}_\ell^{\text{den}} = \mathbf{W}_{\ell,\ell}^{\text{IP}} \varphi(\check{\mathbf{u}}_\ell^P). \quad (28)$$

The nudging currents for the interneurons are $\mathbf{i}^{\text{nudge,I}} = g^{\text{nudge,I}}(\check{\mathbf{u}}_{\ell+1}^{\text{P}} - \check{\mathbf{u}}_{\ell}^{\text{I}})$, and the output layer pyramidal neurons receive a weak instructive signal via $\mathbf{i}^{\text{nudge,tgt}} = g^{\text{nudge,tgt}}(\mathbf{u}^{\text{tgt}} - \check{\mathbf{u}}_N^{\text{P}})$.

In the base microcircuit model of Ref. [8] augmented with prospective coding [9], synaptic plasticity of forward and lateral weights is defined as

$$\dot{\mathbf{W}}_{\ell,\ell-1}^{\text{PP}} = \eta_{\ell}^{\text{fw}} \left[\varphi(\check{\mathbf{u}}_{\ell}^{\text{P}}) - \varphi\left(\frac{g^{\text{bas}}}{g_1 + g^{\text{bas}} + g^{\text{api}}} \mathbf{v}_{\ell}^{\text{bas}}\right) \right] \varphi(\check{\mathbf{u}}_{\ell-1}^{\text{P}})^T \quad \forall \ell \neq N, \quad (29)$$

$$\dot{\mathbf{W}}_{N,N-1}^{\text{PP}} = \eta_N^{\text{fw}} \left[\varphi(\check{\mathbf{u}}_N^{\text{P}}) - \varphi\left(\frac{g^{\text{bas}}}{g_1 + g^{\text{bas}}} \mathbf{v}_N^{\text{bas}}\right) \right] \varphi(\check{\mathbf{u}}_{N-1}^{\text{P}})^T, \quad (30)$$

$$\dot{\mathbf{W}}_{\ell,\ell}^{\text{IP}} = \eta^{\text{IP}} \left[\varphi(\check{\mathbf{u}}_{\ell}^{\text{I}}) - \varphi\left(\frac{g^{\text{den}}}{g_1 + g^{\text{den}}} \mathbf{v}_{\ell}^{\text{den}}\right) \right] \varphi(\check{\mathbf{u}}_{\ell}^{\text{P}})^T, \quad (31)$$

$$\dot{\mathbf{B}}_{\ell,\ell}^{\text{PI}} = \eta_{\ell}^{\text{PI}} \left[-\mathbf{v}_{\ell}^{\text{api}} \right] \varphi(\check{\mathbf{u}}_{\ell}^{\text{I}})^T, \quad (32)$$

while top-down weights $\mathbf{B}_{\ell,\ell+1}^{\text{PP}}$ are fixed.

Before deriving the relevant analytical expressions, we briefly explain how the design of the circuitry leads to well-defined error propagation. In absence of a teaching signal, and if the microcircuit has settled into its self-predicting state, the interneuron activity in each layer represents an exact copy of the pyramidal neurons in the layer above. Interneurons project laterally onto the apical dendrites of pyramidal cells in the same layer; these apical dendrites also receive input from pyramidal cells in the layer above. In the self-predicting state, these activities are subtracted from each other; as they are exactly the same, the inputs cancel, and the apical compartment voltage is zero.

We now introduce a weak nudging signal towards the correct voltage at the output layer. To first order in expansion parameters, the interneurons still represent the pyramidal neurons in the layer above *in absence of a teaching signal*. The activity of the pyramidal cell in the layer above now however additionally contains the error signal. Therefore, the difference in activity calculated at the apical dendrite in a given layer also represents an error. Starting from the penultimate layer, this argument extends successively to the apical compartment voltages in all hidden layers. Consequently, the apical compartments represent errors useful for learning, and these errors are backpropagated.

In order to prove the above statements, we reconsider the dynamics defined by Eqs. (23)–(25) without noise, and learning rules (29)–(32). Before performing supervised training, the system must settle in a self-predicting state. This is achieved by presenting input sequences while clamping the target voltage to the prospective voltage, $\mathbf{u}^{\text{tgt}} = \check{\mathbf{u}}_N^{\text{P}}$, and evolving the system while keeping the bottom-up weights $\mathbf{W}_{\ell+1,\ell}^{\text{PP}}$ and top-down weights $\mathbf{B}_{\ell,\ell+1}^{\text{PP}}$ fixed. The dynamics of the lateral weights, $\dot{\mathbf{W}}_{\ell,\ell}^{\text{IP}}$ and $\dot{\mathbf{B}}_{\ell,\ell}^{\text{PI}}$, are designed to drive the respective weights to the self-predicting state and are required to work in conjunction.

The lateral connections from interneurons to pyramidal cells $\mathbf{B}_{\ell,\ell}^{\text{PI}}$ are driven by gradient descent on the mismatch energy $\|\mathbf{v}_{\ell}^{\text{api}}\|^2$ defined by the apical compartment potential. For fixed top-down synapses, the dynamics of Eq. (32) settle such that $\mathbf{v}_{\ell}^{\text{api}}$ is (approximately) zero for all inputs.

Through the dynamics of Eq. (31), the weights $\mathbf{W}_{\ell,\ell}^{\text{IP}}$ are adapted to minimize the difference between the dendritic potential of the interneurons and the voltage in the basal compartment of pyramidal cells in the layer above. This can be seen by expanding the learning rule in

$$g^{\text{nudge,I}} \ll g_1 + g^{\text{den}},$$

$$\dot{\mathbf{W}}_{\ell,\ell}^{\text{IP}} \propto \varphi(\check{\mathbf{u}}_\ell^{\text{I}}) - \varphi\left(\frac{g^{\text{den}}}{g_1 + g^{\text{den}}} \mathbf{v}_\ell^{\text{den}}\right) \quad (33)$$

$$= \varphi\left(\frac{g^{\text{den}} \mathbf{v}_\ell^{\text{den}} + g^{\text{nudge,I}} \check{\mathbf{u}}_{\ell+1}^{\text{P}}}{g_1 + g^{\text{den}} + g^{\text{nudge,I}}}\right) - \varphi\left(\frac{g^{\text{den}}}{g_1 + g^{\text{den}}} \mathbf{v}_\ell^{\text{den}}\right) \quad (34)$$

$$\approx \varphi'\left(\frac{g^{\text{den}}}{g_1 + g^{\text{den}}} \mathbf{v}_\ell^{\text{den}}\right) \frac{g^{\text{nudge,I}}}{g_1 + g^{\text{den}}} \left[\check{\mathbf{u}}_{\ell+1}^{\text{P}} - \frac{g^{\text{den}}}{g_1 + g^{\text{den}}} \mathbf{v}_\ell^{\text{den}}\right], \quad (35)$$

where in the first step, we have replaced the prospective interneuron voltage with the potentials which induce it, $\check{\mathbf{u}}_\ell^{\text{I}} = \frac{g^{\text{den}} \mathbf{v}_\ell^{\text{den}} + g^{\text{nudge,I}} \check{\mathbf{u}}_{\ell+1}^{\text{P}}}{g_1 + g^{\text{den}} + g^{\text{nudge,I}}}$ given by Eq. (25). In the second step, we expand in weak nudging of the interneuron.

In conjunction with the minimization of the apical potential in all layers through $\dot{\mathbf{B}}_{\ell,\ell}^{\text{PI}}$, the prospective potential $\check{\mathbf{u}}_{\ell+1}^{\text{P}}$ is fully determined by its basal input, $\check{\mathbf{u}}_{\ell+1}^{\text{P}} = \frac{g^{\text{bas}}}{g_1 + g^{\text{bas}} + g^{\text{api}}} \mathbf{v}_{\ell+1}^{\text{bas}}$ for $1 \leq \ell < N - 1$ and $\check{\mathbf{u}}_N^{\text{P}} = \frac{g^{\text{bas}}}{g_1 + g^{\text{bas}}} \mathbf{v}_N^{\text{bas}}$ for the output layer. Therefore, the synapses settle into a state which minimizes the difference between the basal voltage $\mathbf{v}_{\ell+1}^{\text{bas}}$ and the interneuron compartment $\mathbf{v}_\ell^{\text{den}}$ (up to a factor defined by the conductances) for all input samples.

After the lateral weights have converged, the interneuron potentials are an exact copy of the pyramidal cells in the layer above, $\check{\mathbf{u}}_\ell^{\text{I}} = \check{\mathbf{u}}_{\ell+1}^{\text{P}}$; this can be seen by plugging the steady state solution $g^{\text{den}} \mathbf{v}_\ell^{\text{den}} = (g_1 + g^{\text{den}}) \check{\mathbf{u}}_{\ell+1}^{\text{P}}$ into the expression of $\check{\mathbf{u}}_\ell^{\text{I}}$ in terms of its compartmental voltages.

A particularly well-suited self-predicting state is defined by

$$\begin{aligned} \mathbf{B}_{\ell,\ell}^{\text{PI}} &= -\mathbf{B}_{\ell,\ell+1}^{\text{PP}} \\ \mathbf{W}_{\ell,\ell}^{\text{IP}} &= \frac{g^{\text{bas}}}{g^{\text{den}}} \frac{g_1 + g^{\text{den}}}{g_1 + g^{\text{bas}} + g^{\text{api}}} \mathbf{W}_{\ell+1,\ell}^{\text{PP}} \end{aligned} \quad (36)$$

for hidden layers, and $\mathbf{W}_{N-1,N-1}^{\text{IP}} = \frac{g^{\text{bas}}}{g^{\text{den}}} \frac{g_1 + g^{\text{den}}}{g_1 + g^{\text{bas}}} \mathbf{W}_{N,N-1}^{\text{PP}}$ for the lateral weights projecting to the interneurons in the final hidden layer. This state has the advantage that the lateral weights form a self-predicting state independent of the input data (general solutions of $\dot{\mathbf{W}}_{\ell,\ell}^{\text{IP}} = 0 = \dot{\mathbf{B}}_{\ell,\ell}^{\text{PI}}$ do not perform as well in practice, as stimulus switching often requires re-learning of lateral weights before apical compartments represent useful error signal). In the simulations presented in this work, the networks are initialized in this specific self-predicting state.

We now turn on a teaching signal \mathbf{u}^{tgt} . The new, nudged prospective state of the output neurons is $\check{\mathbf{u}}_N^{\text{P}} = \frac{g^{\text{bas}} \mathbf{v}_N^{\text{bas}} + g^{\text{nudge,tgt}} \mathbf{u}^{\text{tgt}}}{g_1 + g^{\text{bas}} + g^{\text{nudge,tgt}}}$. Inserting this state into Eq. (30) and expanding the somatic potential about the weighted basal input $\hat{\mathbf{v}}_N^{\text{bas}}$, we obtain

$$\Delta \mathbf{W}_{N,N-1}^{\text{PP}} \approx \varphi'(\hat{\mathbf{v}}_N^{\text{bas}}) \cdot \frac{g^{\text{nudge,tgt}}}{g_1 + g^{\text{bas}} + g^{\text{nudge,tgt}}} [\mathbf{u}^{\text{tgt}} - \hat{\mathbf{v}}_N^{\text{bas}}] (\mathbf{r}_{N-1}^{\text{P}})^T. \quad (37)$$

Here, we have defined $\hat{\mathbf{v}}_N^{\text{bas}} := \frac{g^{\text{bas}}}{g_1 + g^{\text{bas}}} \mathbf{v}_N^{\text{bas}}$, and we have rewritten the bottom-up input from pyramidal neurons in the penultimate layer as a rate $\mathbf{r}_{N-1}^{\text{P}}$. We can now identify the difference between target and bottom-up input as the output layer error, $\mathbf{e}_N := \mathbf{u}^{\text{tgt}} - \hat{\mathbf{v}}_N^{\text{bas}}$, and we may thus write

$$\Delta \mathbf{W}_{N,N-1}^{\text{PP}} \propto \varphi'(\hat{\mathbf{v}}_N^{\text{bas}}) \mathbf{e}_N (\mathbf{r}_{N-1}^{\text{P}})^T. \quad (38)$$

Written in this form, we have demonstrated that the update rule (30) implements error minimization on the output layer in the limit of weak nudging. One can regard this as equivalent to training the output layer of a feed-forward network, evaluated at the weighted input $\hat{\mathbf{v}}_N^{\text{bas}}$.

We now aim to show that the error \mathbf{e}_N is propagated backwards through the network, where the apical compartment voltages represent the local error within each layer. Starting from the self-predicting state, the apical voltages are

$$\begin{aligned} \mathbf{v}_{N-1}^{\text{api}} &= \mathbf{B}_{N-1,N}^{\text{PP}} [\varphi(\check{\mathbf{u}}_N^{\text{P}}) - \varphi(\check{\mathbf{u}}_{N-1}^{\text{I}})] \\ &= \mathbf{B}_{N-1,N}^{\text{PP}} \left[\varphi \left(\frac{g^{\text{bas}} \mathbf{v}_N^{\text{bas}} + g^{\text{nudge,tgt}} \mathbf{u}^{\text{tgt}}}{g_1 + g^{\text{bas}} + g^{\text{nudge,tgt}}} \right) - \varphi \left((1 - \lambda^{\text{I}}) \hat{\mathbf{v}}_N^{\text{bas}} + \lambda^{\text{I}} \frac{g^{\text{bas}} \mathbf{v}_N^{\text{bas}} + g^{\text{nudge,tgt}} \mathbf{u}^{\text{tgt}}}{g_1 + g^{\text{bas}} + g^{\text{nudge,tgt}}} \right) \right] \end{aligned} \quad (39)$$

$$\begin{aligned} \mathbf{v}_\ell^{\text{api}} &= \mathbf{B}_{\ell,\ell+1}^{\text{PP}} [\varphi(\check{\mathbf{u}}_{\ell+1}^{\text{P}}) - \varphi(\check{\mathbf{u}}_\ell^{\text{I}})] \\ &= \mathbf{B}_{\ell,\ell+1}^{\text{PP}} \left[\varphi \left(\hat{\mathbf{v}}_{\ell+1}^{\text{bas}} + \lambda^{\text{P}} \mathbf{v}_{\ell+1}^{\text{api}} \right) - \varphi \left(\hat{\mathbf{v}}_{\ell+1}^{\text{bas}} + \lambda^{\text{I}} \lambda^{\text{P}} \mathbf{v}_{\ell+1}^{\text{api}} \right) \right] \end{aligned} \quad (40)$$

with $\lambda^{\text{I}} := \frac{g^{\text{nudge,I}}}{g_1 + g^{\text{den}} + g^{\text{nudge,I}}}$, $\lambda^{\text{P}} := \frac{g^{\text{api}}}{g_1 + g^{\text{bas}} + g^{\text{api}}}$, and $\hat{\mathbf{v}}_{\ell+1}^{\text{bas}} := \frac{g^{\text{bas}}}{g_1 + g^{\text{bas}} + g^{\text{api}}} \mathbf{v}_{\ell+1}^{\text{bas}}$. Let us first focus on the apical voltage in the penultimate layer. We again make use of the assumption of weak nudging, and additionally require that the interneuron is only weakly nudged by the top-down input it receives, $\lambda^{\text{I}} \ll 1$. The apical voltage takes the form

$$\mathbf{v}_{N-1}^{\text{api}} \approx \mathbf{B}_{N-1,N}^{\text{PP}} \varphi' \left(\hat{\mathbf{v}}_N^{\text{bas}} \right) \frac{g^{\text{nudge,tgt}}}{g_1 + g^{\text{bas}}} \mathbf{e}_N. \quad (41)$$

In the same fashion, we expand the apical potentials in the layers below. The first order in $\lambda^{\text{P}} \mathbf{v}_{\ell+1}^{\text{api}}$ and zeroth order in λ^{I} yields

$$\mathbf{v}_\ell^{\text{api}} \approx \mathbf{B}_{\ell,\ell+1}^{\text{PP}} \varphi' \left(\hat{\mathbf{v}}_{\ell+1}^{\text{bas}} \right) \lambda^{\text{P}} \mathbf{v}_{\ell+1}^{\text{api}}. \quad (42)$$

Taken together, these two results show that the apical potentials represent errors which are successively propagated backwards through the network.

Finally, the last missing ingredient is how apical errors are used to update the forward weights. Performing the same expansion in small apical voltages on Eq. (29), we obtain

$$\Delta \mathbf{W}_{\ell,\ell-1}^{\text{PP}} \propto \lambda^{\text{P}} \varphi'(\hat{\mathbf{v}}_\ell^{\text{bas}}) \mathbf{v}_\ell^{\text{api}} (\mathbf{r}_{\ell-1}^{\text{P}})^T. \quad (43)$$

We now collect and summarize our findings. Bottom-up weights $\mathbf{W}_{\ell,\ell-1}^{\text{PP}}$ are updated using the local error, represented by the apical voltage as $\mathbf{v}_\ell^{\text{api}}$, multiplied with the bottom-up signal $\mathbf{r}_{\ell-1}^{\text{P}}$. Eqs. (41) and (42) show that these errors are backpropagated by multiplying with the derivative $\varphi'(\hat{\mathbf{v}}_{\ell+1}^{\text{bas}})$ and feedback weights $\mathbf{B}_{\ell,\ell+1}^{\text{PP}}$. This learning scheme resembles that of feed-forward networks trained with feedback alignment (for fixed \mathbf{B}^{PP}), or backpropagation (if $\mathbf{B}_{\ell,\ell+1}^{\text{PP}} = (\mathbf{W}_{\ell+1,\ell}^{\text{PP}})^T$). One marked difference to a feed-forward network is the emergence of the derivative $\varphi'(\hat{\mathbf{v}}_N^{\text{bas}})$ in the update rule to all bottom-up weights, see Eq. (38) and (41). As we have defined the error \mathbf{e}_N on the voltage level, one may expect there to be no such derivative, as one finds in the corresponding case of a feed-forward networks trained with backpropagation with linear activation functions on the output layer. This additional factor signals a fundamental difference in architecture between backpropagation and difference target propagation, of which dendritic cortical microcircuits are an implementation. In difference target propagation, targets are constructed locally from backpropagated rates – i.e. a target potential \mathbf{u}^{tgt} is converted into a rate before it can be passed to a lower layer. In contrast, in backpropagation, top-down signals

are given by errors, bypassing the activation function in the upper layer and instead directly transporting potential differences to hidden layers.

We now incorporate this result with PAL. As shown in Eq. (14) in App. A.1, using PAL, the top-down weights converge to $\mathbb{E}[\mathbf{B}_{\ell,\ell+1}] \propto \varphi'(\check{\mathbf{u}}_\ell^0) [\mathbf{W}_{\ell+1,\ell}]^T \varphi'(\check{\mathbf{u}}_{\ell+1}^0) \forall \ell$. In the microcircuit model, forward weights are learned as derived in Eq. (43); in summary, we have found that

$$\Delta \mathbf{W}_{\ell,\ell-1}^{\text{PP}} \propto \varphi'(\hat{\mathbf{v}}_\ell^{\text{bas}}) \left[\prod_{k=\ell}^{N-1} \mathbf{B}_{k,k+1}^{\text{PP}} \varphi'(\hat{\mathbf{v}}_{k+1}^{\text{bas}}) \right] \mathbf{e}_N (\mathbf{r}_{\ell-1}^{\text{P}})^T. \quad (44)$$

In the limit of weak nudging and feedback, the noise-free potentials $\check{\mathbf{u}}_\ell^{\text{P},0}$ are well approximated by the bottom-up input $\hat{\mathbf{v}}_\ell^{\text{bas}}$, and our result for top-down weights takes the form $\mathbb{E}[\mathbf{B}_{\ell,\ell+1}^{\text{PP}}] \propto \varphi'(\hat{\mathbf{v}}_\ell^{\text{bas}}) [\mathbf{W}_{n+1,n}^{\text{PP}}]^T \varphi'(\hat{\mathbf{v}}_{\ell+1}^{\text{bas}}) \forall \ell$. Plugging this into Eq. (44), we see that the weight updates $\Delta \mathbf{W}_{\ell,\ell-1}^{\text{PP}}$ align with those of a feed-forward network trained with backpropagation up to additional factors of derivatives. Therefore, our algorithm can provide useful error signals which approximately align with backpropagation, improving on random feedback weights.

A.3 Local alignment is compatible with approximate Gauss Newton-target propagation

The framework of PAL can easily be extended to propagate Gauss-Newton targets. As shown in Ref. [24], this requires the training of feedback connections such that they invert the signal passed from given layer ℓ to the output layer N ; i.e. training weights such that the backward mapping Jacobian matrix $\mathbf{J}_{g_{\ell,N}}$ is a pseudoinverse of the forward mapping, $\mathbf{J}_{g_{\ell,N}} = [\mathbf{J}_{f_{N,\ell}}]^+$. These feedback mappings could be realized by skip connections from the output layer to each hidden layer, while maintaining a layer-wise feed-forward architecture. In contrast to the layer-wise feedback setup defined in the main text (cf. Fig. 2), only one interneuron population matching the output layer pyramidal cells would be required here, as the same error signal \mathbf{e}_N is backpropagated to all hidden layers.

In analogy to DTP-DRL [24], we can define a difference-based reconstruction loss,

$$\mathcal{L}_\ell^{\text{diff}} = \|\mathbf{B}_{\ell,N} \hat{\mathbf{r}}_N - \boldsymbol{\xi}_\ell\|^2 + \alpha \|\mathbf{B}_{\ell,N}\|^2. \quad (45)$$

Gradient descent on this reconstruction loss yields the update rule

$$\dot{\mathbf{B}}_{\ell,N} = -\eta_i^{\text{bw}} [(\mathbf{B}_{\ell,N} \hat{\mathbf{r}}_N - \boldsymbol{\xi}_\ell) \hat{\mathbf{r}}_N + \alpha \mathbf{B}_{\ell,N}]. \quad (46)$$

If noise injection and plasticity of top-down weights is phased, i.e. by a schedule that sequentially injects noise only into a given layer ℓ while enabling plasticity of $\mathbf{B}_{\ell,N}$, this learning rule minimizes the reconstruction loss of $\boldsymbol{\xi}_\ell$ as it passes to the output layer and back. This can be seen by plugging in the equivalent of Eq. (6) for phased noise,

$$\hat{\mathbf{r}}_N \approx \varphi'(\check{\mathbf{u}}_N^0) \left[\prod_{n=\ell}^{N-1} \mathbf{W}_{n+1,n} \varphi'(\check{\mathbf{u}}_n^0) \right] \boldsymbol{\xi}_\ell. \quad (47)$$

The difference $\mathbf{B}_{\ell,N} \hat{\mathbf{r}}_N - \boldsymbol{\xi}_\ell$ is minimal if $\mathbf{B}_{\ell,N} \varphi'(\check{\mathbf{u}}_N^0)$ is equal to $\lambda^{\text{P}} \left[\prod_{n=\ell}^{N-1} \mathbf{W}_{n+1,n}^{\text{PP}} \varphi'(\check{\mathbf{u}}_n^0) \right]^+$, thereby aligning the backwards Jacobian with the Moore-Penrose inverse of the forward Jacobian matrix.

As shown in Ref. [24], learning backwards weight to minimize such a reconstruction loss produces forward updates closely related to Gauss-Newton optimization,

$$\Delta \mathbf{W}_{\ell, \ell-1}^{\text{PP}} \propto [\mathbf{J}_{f_{N, \ell}}]^+ \mathbf{e}_N (\mathbf{r}_{\ell-1}^{\text{P}})^T, \quad (48)$$

where $\mathbf{J}_{f_{N, \ell}}$ denotes the Jacobian matrix mapping potentials in layer ℓ to the output layer N .

While error propagation using the Moore-Penrose inverse has been shown to perform well on simple classification tasks [23, 24, 36, 75], it is currently not known how such a difference reconstruction loss could be implemented while training all top-down weights simultaneously.

B Simulation of PAL

B.1 Microcircuit models

Below we address several implementation details:

For all simulations, we set the resting potential to $\mathbf{E}_1 = 0$. Effective time constants are calculated as the ratio of dimensionless conductances (setting the capacitance to 1): $\tau_{\ell}^{\text{eff, P}} = \frac{1}{g_1 + g^{\text{bas}} + g^{\text{api}}}$ for pyramidal neurons in hidden layers; $\tau_N^{\text{eff, P}} = \frac{1}{g_1 + g^{\text{bas}} + g^{\text{nudge, tgt}}}$ for output layer neurons in presence of a nudging signal; $\tau_N^{\text{eff, P}} = \frac{1}{g_1 + g^{\text{bas}}}$ for output layer neurons in absence of a nudging signal; $\tau_{\ell}^{\text{eff, I}} = \frac{1}{g_1 + g^{\text{den}} + g^{\text{nudge, I}}}$ for interneurons.

Fig. 3 (Phaseless backwards weight alignment): In order to compare the backprojections with those in an ANN trained with BP (right column), we perform several steps. After each epoch of top-down weight training, we instantiate a teacher model with the architecture as the respective ‘student’ microcircuit model. To this model, we pass the input sequence and record the teacher output as a target signal. We now provide the newly acquired input/target pairs to the student model. As in all other simulations, these pairs are presented for $T_{\text{pres}} = 100 dt$, and we disable noise during this evaluation. It is also necessary to set the lateral weights to the self-predicting state defined by Eqs. (36) in order to obtain a measurable error signal in layers below the last hidden layer. We record the potential weight updates defined by the backprojections, but do not apply them.

Next, we feed the same input/target sequence into an ANN with weights set to $\mathbf{W}_{\ell, \ell-1}^{\text{PP}}$ and layer size and activation as defined in Tab. 1. For this ANN, we calculate the output layer error as the difference between target and voltage (linear activation on output layer). The weight update given in this ANN is then compared to the recorded update for the microcircuit model.

Fig. 4 (Teacher-student setup): We initialize the teacher with weights $\mathbf{W}_{2,1}^{\text{PP}} = \mathbf{W}_{1,0}^{\text{PP}} = 2$. For the student models with feedback alignment, the same parameters as for PAL are used, but with $\eta^{\text{bw}} = \eta^{\text{PI}} = 0$, no noise injection, and without the low-pass filter on $\Delta \mathbf{W}_{\ell, \ell-1}^{\text{PP}}$. For the BP reference model, we additionally set $\mathbf{B}_{\ell-1, \ell}^{\text{PP}} = [\mathbf{W}_{\ell, \ell-1}^{\text{PP}}]^T$ and $\mathbf{B}_{\ell-1, \ell}^{\text{PI}} = -\mathbf{B}_{\ell-1, \ell}^{\text{PP}}$ after every update.

Fig. 4 (Classification tasks): For the Yin-Yang task, we used datasets of size 6 000 for training, 900 for validation, and 900 for testing. For MNIST digit classification, sets were 50 000 for training, 10 000 for validation, and 10 000 for testing. In either case, FA runs use the same parameters as PAL, but with fixed $\mathbf{B}_{\ell, \ell+1}^{\text{PP}}$ and $\mathbf{B}_{\ell, \ell}^{\text{PI}}$ and no noise injection. The reference network is an ANN trained with BP using a Cross-Entropy loss and ADAM with default parameters of PyTorch. In this case, 10 seeds were trained.

Algorithm 1: Dendritic cortical microcircuits with prospective coding and PAL

Input: Data stream encoded as rate vector $\mathbf{r}_0^{\text{P}}[t]$, target voltage vector $\mathbf{u}^{\text{tgt}}[t]$
Parameters: Network with layers 1 to N ; effective neuron time constants $\tau_{\ell}^{\text{eff,P}}, \tau_{\ell}^{\text{eff,I}}$

- 1 **Update instantaneous rates and compartment potentials**
- 2 **for** ℓ *in range*(1, N) **do**
- 3 $\check{\mathbf{u}}_{\ell}^{\text{P}}[t] \leftarrow \mathbf{u}_{\ell}^{\text{P}}[t - dt] + \frac{\tau_{\ell}^{\text{eff,P}}}{dt} (\mathbf{u}_{\ell}^{\text{P}}[t] - \mathbf{u}_{\ell}^{\text{P}}[t - dt])$
- 4 $\check{\mathbf{u}}_{\ell}^{\text{I}}[t] \leftarrow \mathbf{u}_{\ell}^{\text{I}}[t - dt] + \frac{\tau_{\ell}^{\text{eff,I}}}{dt} (\mathbf{u}_{\ell}^{\text{I}}[t] - \mathbf{u}_{\ell}^{\text{I}}[t - dt])$
- 5 $\mathbf{r}_{\ell}^{\text{P}}[t] \leftarrow \varphi(\check{\mathbf{u}}_{\ell}^{\text{P}}[t])$
- 6 $\mathbf{r}_{\ell}^{\text{I}}[t] \leftarrow \varphi(\check{\mathbf{u}}_{\ell}^{\text{I}}[t])$
- 7 **for** ℓ *in range*(1, N) **do**
- 8 $\mathbf{v}_{\ell}^{\text{bas}}[t] \leftarrow \mathbf{W}_{\ell,\ell-1}^{\text{PP}}[t] \mathbf{r}_{\ell-1}^{\text{P}}[t]$
- 9 $\mathbf{v}_{\ell}^{\text{api}}[t] \leftarrow \mathbf{B}_{\ell,\ell+1}^{\text{PP}}[t] \mathbf{r}_{\ell+1}^{\text{P}}[t] + \mathbf{B}_{\ell,\ell}^{\text{PI}}[t] \mathbf{r}_{\ell}^{\text{I}}[t]$
- 10 $\mathbf{v}_{\ell}^{\text{den}}[t] \leftarrow \mathbf{W}_{\ell,\ell}^{\text{IP}}[t] \mathbf{r}_{\ell}^{\text{P}}[t]$
- 11 **Update high-pass filtered rates**
- 12 **for** ℓ *in range*(1, N) **do**
- 13 $\hat{\mathbf{r}}_{\ell}^{\text{P}}[t] \leftarrow \hat{\mathbf{r}}_{\ell}^{\text{P}}[t - dt] + \mathbf{r}_{\ell}^{\text{P}}[t] - \mathbf{r}_{\ell}^{\text{P}}[t - dt] - \frac{dt}{\tau_{\text{hp}}} \hat{\mathbf{r}}_{\ell}^{\text{P}}[t - dt]$
- 14 **Update noise vectors**
- 15 **for** ℓ *in range*(1, $N - 1$) **do**
- 16 $\boldsymbol{\mu}_{\ell} \sim \mathcal{N}(0, \mathbb{I})$
- 17 $\boldsymbol{\xi}_{\ell}[t] \leftarrow \boldsymbol{\xi}_{\ell}[t - dt] + \frac{1}{\tau_{\xi}} (\sqrt{\tau_{\xi} dt} \sigma_{\ell} \boldsymbol{\mu}_{\ell} - dt \boldsymbol{\xi}_{\ell}[t - dt])$
- 18 **Update somatic potentials with noise injection**
- 19 **for** ℓ *in range*(1, $N - 1$) **do**
- 20 $\mathbf{u}_{\ell}^{\text{eff,I}}[t] \leftarrow \tau_{\ell}^{\text{eff,I}} \{g^{\text{den}} \mathbf{v}_{\ell}^{\text{den}}[t] + g^{\text{nudge,I}} \check{\mathbf{u}}_{\ell+1}^{\text{P}}[t]\}$
- 21 $\Delta \mathbf{u}_{\ell}^{\text{I}}[t] \leftarrow \frac{dt}{\tau_{\ell}^{\text{eff,I}}} \{\mathbf{u}_{\ell}^{\text{eff,I}}[t] - \mathbf{u}_{\ell}^{\text{I}}[t]\}$
- 22 $\mathbf{u}_{\ell}^{\text{eff,P}}[t] \leftarrow \tau_{\ell}^{\text{eff,P}} \{g^{\text{bas}} \mathbf{v}_{\ell}^{\text{bas}}[t] + g^{\text{api}} (\mathbf{v}_{\ell}^{\text{api}}[t] + \boldsymbol{\xi}_{\ell}[t])\}$
- 23 $\Delta \mathbf{u}_{\ell}^{\text{P}}[t] \leftarrow \frac{dt}{\tau_{\ell}^{\text{eff,P}}} \{\mathbf{u}_{\ell}^{\text{eff,P}}[t] - \mathbf{u}_{\ell}^{\text{P}}[t]\}$
- 24 $\mathbf{u}_N^{\text{eff,P}}[t] \leftarrow \tau_N^{\text{eff,P}} \{g^{\text{bas}} \mathbf{v}_N^{\text{bas}}[t] + g^{\text{nudge,tgt}} \mathbf{u}^{\text{tgt}}[t]\}$
- 25 $\Delta \mathbf{u}_N^{\text{P}}[t] \leftarrow \frac{dt}{\tau_N^{\text{eff,P}}} \{\mathbf{u}_N^{\text{eff,P}}[t] - \mathbf{u}_N^{\text{P}}[t]\}$
- 26 apply voltage updates: $\mathbf{u}_{\ell}^{\text{P}} + \Delta \mathbf{u}_{\ell}^{\text{P}}, \mathbf{u}_{\ell}^{\text{I}} + \Delta \mathbf{u}_{\ell}^{\text{I}} \quad \forall \ell$
- 27 **Update weights, incl. low-pass filtering feedforward weight updates**
- 28 **for** ℓ *in range*(1, $N - 1$) **do**
- 29 $\Delta \mathbf{W}_{\ell,\ell-1}^{\text{PP}} \leftarrow dt \eta_{\ell}^{\text{fw}} \{\mathbf{r}_{\ell}^{\text{P}}[t] - \varphi(\frac{g^{\text{bas}}}{g_1 + g^{\text{bas}} + g^{\text{api}}} \mathbf{v}_{\ell}^{\text{bas}}[t - dt])\} \mathbf{r}_{\ell-1}^{\text{P}}[t - dt]$
- 30 $\Delta \mathbf{B}_{\ell,\ell+1}^{\text{PP}} \leftarrow dt \eta_{\ell}^{\text{bw}} \{\boldsymbol{\xi}_{\ell}[t] \hat{\mathbf{r}}_{\ell+1}^{\text{P}}[t - dt] - \alpha_{\ell} \mathbf{B}_{\ell,\ell+1}^{\text{PP}}[t]\}$
- 31 $\Delta \mathbf{B}_{\ell,\ell}^{\text{PI}} \leftarrow -dt \eta_{\ell}^{\text{PI}} \mathbf{v}_{\ell}^{\text{api}}[t - dt] \mathbf{r}_{\ell}^{\text{I}}[t - dt]$
- 32 $\Delta \mathbf{W}_{\ell,\ell}^{\text{IP}} \leftarrow dt \eta_{\ell}^{\text{IP}} \{\mathbf{r}_{\ell}^{\text{I}}[t] - \varphi(\frac{g^{\text{den}}}{g_1 + g^{\text{den}}} \mathbf{v}_{\ell}^{\text{den}}[t - dt])\} \mathbf{r}_{\ell}^{\text{P}}[t - dt]$
- 33 $\Delta \mathbf{W}_{N,N-1}^{\text{PP}} \leftarrow dt \eta_{\ell}^{\text{fw}} \{\mathbf{r}_N^{\text{P}}[t] - \varphi(\frac{g^{\text{bas}}}{g_1 + g^{\text{bas}}} \mathbf{v}_N^{\text{bas}}[t - dt])\} \mathbf{r}_{N-1}^{\text{P}}[t - dt]$
- 34 **for** ℓ *in range*(1, N) **do**
- 35 $\overline{\Delta \mathbf{W}}_{\ell,\ell-1}^{\text{PP}} \leftarrow \overline{\Delta \mathbf{W}}_{\ell,\ell-1}^{\text{PP}}[t - dt] + \frac{dt}{\tau_{\text{lo}}} (\Delta \mathbf{W}_{\ell,\ell-1}^{\text{PP}}[t - dt] - \overline{\Delta \mathbf{W}}_{N,N-1}^{\text{PP}}[t - dt])$
- 36 apply weight updates:
 $\mathbf{W}_{\ell,\ell-1}^{\text{PP}} + \overline{\Delta \mathbf{W}}_{\ell,\ell-1}^{\text{PP}}, \mathbf{B}_{\ell,\ell+1}^{\text{PP}} + \Delta \mathbf{B}_{\ell,\ell+1}^{\text{PP}}, \mathbf{B}_{\ell,\ell}^{\text{PI}} + \Delta \mathbf{B}_{\ell,\ell}^{\text{PI}}, \mathbf{W}_{\ell,\ell}^{\text{IP}} + \Delta \mathbf{W}_{\ell,\ell}^{\text{IP}} \quad \forall \ell$

Table 1: Parameters for microcircuit model simulations.

	Fig. 3 (a+b+c)	Fig. 3 (d+e+f)	Fig. 4 (a+b)	Fig. 4 (c+d)	Fig. 4 (e+f)
dt [ms]	10^{-2}	10^{-2}	10^{-2}	10^{-2}	10^{-2}
T_{pres} [ms]	1	1	1	1	1
τ_{hp} [ms]	0.1	0.1	0.1	0.1	0.1
τ_{lo} [ms]	— [†]	— [†]	10^2	10^2	10^2
τ_{ξ} [ms]	0.1	0.1	0.1	0.1	0.1
noise scale $\sigma_{\ell} \forall \ell$	5×10^{-2}	5×10^{-2}	10^{-2}	10^{-2}	10^{-2}
regularizer α	10^{-5}	10^{-5}	10^{-6}	10^{-6}	10^{-6}
g_l [ms^{-1}]	0.03	0.03	0.03	0.03	0.03
g^{bas} [ms^{-1}]	0.1	0.1	0.1	0.1	0.1
g^{api} [ms^{-1}]	0.06	0.06	0.06	0.06	0.06
g^{den} [ms^{-1}]	0.1	0.1	0.1	0.1	0.1
$g^{\text{nudge, I}}$ [ms^{-1}]	0.06	0.06	0.06	0.06	0.06
$g^{\text{nudge, tgt}}$ [ms^{-1}]	0.06	0.06	0.06	0.06	0.06
input	$\mathcal{U}[0, 1]$	$\mathcal{U}[0, 1]$	$\mathcal{U}[0, 1]$	Yin-Yang	MNIST
dataset size	100	100	100	6 000	50 000
epochs	100	500	5 000	400	100
network size	[5-20-10-20-5]	[5-20-10-20-5]	[1-1-1]	[4-30-3]	[784-100-10]
activation	$\frac{1}{1+e^{-x}}$	$\frac{1}{1+e^{-x}}$	$\frac{1}{1+e^{-x}}$	$\frac{1}{1+e^{-x}}$	$\frac{1}{1+e^{-x}}$
η^{fw} [ms^{-1}]	0, 0, 0, 0	0, 0, 0, 0	2, 0.5	50, 0.01	$1.0, 5 \times 10^{-3}$
η^{bw} [ms^{-1}]	50, 50, 50	20, 20, 20	20	0.5	0.2
η^{IP} [ms^{-1}]	0, 0, 0	0, 0, 0	10	0.05	0.02
η^{PI} [ms^{-1}]	5, 5, 5	0.5, 0.5, 0.5	0.5	0.02	0.02
weight init $\mathbf{W}_{\ell, \ell-1}^{\text{PP}}$	$\mathcal{U}[-1, 1]$	$\mathcal{U}[-5, 5]$	$\mathcal{U}[-1, 0]$	$\mathcal{U}[-0.1, 0.1]$	$\mathcal{U}[-0.1, 0.1]$
weight init $\mathbf{B}_{\ell-1, \ell}^{\text{PP}}$	$\mathcal{U}[-1, 1]$	$\mathcal{U}[-5, 5]$	$\mathcal{U}[-1, 0]$	$\mathcal{U}[-1, 1]$	$\mathcal{U}[-1, 1]$

[†] No forward weight updates applied.

B.2 Efficient credit assignment in deep networks

We detail the parameters for the general LI-model simulation below:

Table 2: Parameters for deep learning simulations of PAL

	Fig. 5	Fig. 6
dt [ms]	10^{-1}	10^{-1}
T_{pres} [ms]	10	10
τ_{hp} [ms]	1	1
τ_{lo} [ms]	— [†]	— [‡]
τ_{ξ} [ms]	1	1
noise scale σ_{ℓ}	$10^{-2} \forall \ell$	$5 \cdot 10^{-2} \forall \ell$
regularizer α	10^{-4}	5×10^{-5}
input	MNIST	CIFAR-10
loss	MSE	MSE
epochs	10	50
batch size	32	128
architecture	Dense: [784-200-2-200-784]	Conv2d((5 × 5) × 20), MaxPool(2) Conv2d((5 × 5) × 50), MaxPool(2) 500 10
activation	tanh, linear, tanh, linear	sigmoid, sigmoid, sigmoid, linear
η^{fw} [ms^{-1}]	$8 \times 10^{-3}, 8 \times 10^{-3}, 8 \times 10^{-3}, 8 \times 10^{-4}$	5, 1, 2, 0.2
η^{bw} [ms^{-1}]	0.8, 0.8, 0.8	0*, 10, 10
weight init $\mathbf{W}_{\ell, \ell-1}$	$\mathcal{N}(0, 0.05)$	$\mathcal{N}(0, 0.05)$
weight init $\mathbf{B}_{\ell-1, \ell}$	$\mathcal{N}(0, 0.05)$	$\mathcal{N}(0, 0.05)$
bias init \mathbf{b}_{ℓ}	$\mathcal{N}(0, 0.05)$	$\mathcal{N}(0, 0.05)$

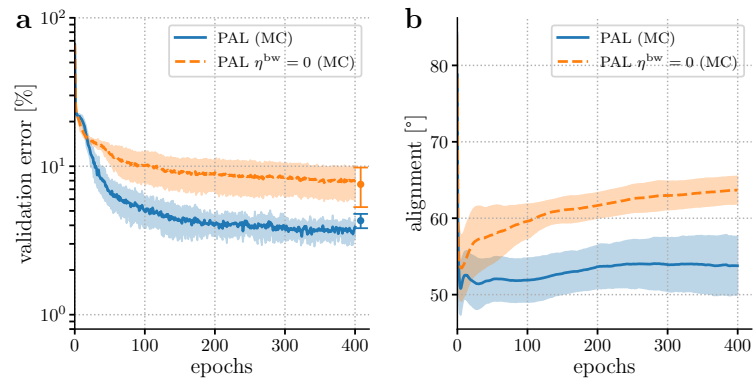
[†] Low-pass filter disabled, as we found no improvement when enabled.

[‡] Noise does not affect top-down errors in this setup (see Methods); thus, low-pass filtering of weights is disabled.

* PAL enabled only for fully connected layers, see Methods.

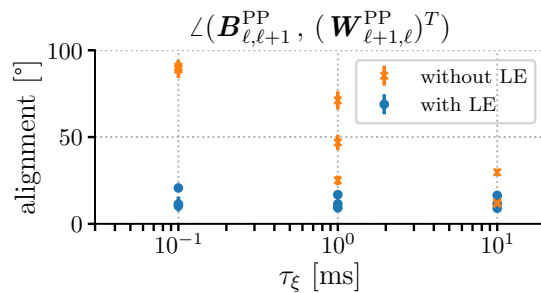
Errors on the output layer are defined as $\mathbf{e}_N = \beta (\mathbf{u}^{\text{tgt}} - \check{\mathbf{u}}_N)$, and we have simulated with $\beta = 0.1$. The dataset sizes for the MNIST autoencoder task are 50 000 for training, 10 000 for validation, and 10 000 for testing. For CIFAR-10, this was 40 000 training images, 10 000 for validation, and 10 000 for testing.

B.3 PAL outperforms FA with noise



Supplementary Figure 2: PAL outperforms FA not simply due to inclusion of noise. A key difference between the experiments performed with PAL and FA is the inherent modeling of noise. Therefore, it could be argued that FA with noise may perform on par with PAL. To test this, we reproduce the Yin-Yang experiment of Fig. 4 (c,d). PAL without learning of top-down weights ($\eta^{bw} = 0$) is equivalent to FA with noise, which performs similar to vanilla FA and is still outperformed by PAL.

B.4 PAL makes full use of prospective coding for efficient weight learning



Supplementary Figure 3: PAL makes full use of prospective coding for efficient weight learning.

The setup of Fig. 3 (a,b,c) is repeated (learning of top-down weights in the microcircuit model) with and without prospective coding (Latent Equilibrium, LE). Shown are the angles between forward and backward weights for all layers after 100 epochs (mean and standard deviation over 10 seeds). In order to learn the correct weights, the model without prospective coding needs to be trained with orders of magnitude larger time constants (the noise time constant τ_ξ needs to be larger than $\tau^{\text{eff,P}} \approx 7$ ms, while $T_{\text{pres}} \gg \tau_\xi$ still holds). Prospective coding therefore represents a leap in efficiency for learning in cortical models with slow neurons. Note that this advantage also translates to practical terms – in this case, wall clock simulation times increased from 10 minutes to 15 hours when disabling prospective coding.